Publications of the Astronomical Society of the Pacific, 130:051001 (18pp), 2018 May https://doi.org/10.1088/1538-3873/aaa8d7

Gamma-ray Burst Prompt Correlations: Selection and Instrumental Effects

M. G. Dainotti[1,2,3] and L. Amati[2]
[1] Physics Department, Stanford University, Via Pueblo Mall 382, Stanford, CA, USA; mdainott@stanford.edu
[2] INAF-Istituto di Astrofisica Spaziale e Fisica cosmica, Via Gobetti 101, 40129,Bologna, Italy
[3] Astronomical Observatory, Jagiellonian University, ul. Orla 171, 31-244 Kraków, Poland; mariagiovannadainotti@yahoo.it
Received 2017 March 24; accepted 2018 January 5; published 2018 April 6

Abstract

The prompt emission mechanism of gamma-ray bursts (GRB) even after several decades remains a mystery. However, it is believed that correlations between observable GRB properties, given their huge luminosity/radiated energy and redshift distribution extending up to at least $z \approx 9$, are promising possible cosmological tools. They also may help to discriminate among the most plausible theoretical models. Nowadays, the objective is to make GRBs standard candles, similar to supernovae (SNe) Ia, through well-established and robust correlations. However, differently from SNe Ia, GRBs span over several order of magnitude in their energetics, hence they cannot yet be considered standard candles. Additionally, being observed at very large distances, their physical properties are affected by selection biases, the so-called Malmquist bias or Eddington effect. We describe the state of the art on how GRB prompt correlations are corrected for these selection biases to employ them as redshift estimators and cosmological tools. We stress that only after an appropriate evaluation and correction for these effects, GRB correlations can be used to discriminate among the theoretical models of prompt emission, to estimate the cosmological parameters and to serve as distance indicators via redshift estimation.

Key words: (stars:) gamma-ray burst: general

Online material: color figure

1. Introduction

Gamma-ray bursts (GRBs), discovered in the late 1960s (Klebesadel et al. 1973), still need further investigation to be fully understood (Kumar & Zhang 2015). From a phenomenological point of view, a GRB is composed of the prompt emission, which consists of high-energy photons such as γ-rays and hard X-rays, and the afterglow emission, i.e., a long-lasting multi-wavelength emission (X-ray, optical, infrared, and sometimes also radio), which follows the prompt. The first afterglow was observed in 1997 by the *BeppoSAX* satellite (Costa et al. 1997; van Paradijs et al. 1997). The X-ray afterglow emission has been studied extensively with the *BeppoSAX*, *XMM-Newton*, and especially with *Swift* (Gehrels et al. 2005), which allowed the discovery of the plateau emission (a flat part in the afterglow soon after the decay phase of the prompt emission) and the phenomenology of the early afterglow.

GRBs are traditionally classified into short (with durations $T_{90} < 2$ s, SGRBs) and long (with $T_{90} > 2$ s, LGRBs) (Mazets et al. 1981; Kouveliotou et al. 1993) depending on their duration. Moreover, the possibility of a third class with intermediate durations was argued some time ago (Horváth 1998; Mukherjee et al. 1998), however counter arguments were recently presented (Zitouni et al. 2015; Tarnopolski 2015a). Another class—short with extended emission with extended emission (SEE-GRBs)—exhibiting properties mixed between SGRBs and LGRBs was discovered by Norris & Bonnell (2006). On the other hand, X-ray Flashes (XRFs; Heise et al. 2001; Kippen et al. 2001), extragalactic transient X-ray sources with properties similar to LGRBs (spatial distribution, spectral, and temporal characteristics), are distinct from GRBs due to having a peak in the νF_ν prompt emission spectrum at energies roughly an order of magnitude smaller than the one observed for regular GRBs and by a fluence in the X-ray band (2–30 keV) greater than in the γ-ray band (30–400 keV). GRB classifications are important for the investigation of GRB correlations, as some of them become more or less evident upon the introduction of different GRB classes (for a discussion, see Amati 2006 and Dainotti et al. 2010). Another important feature of GRB light curves is the variability, V, defined in Section 2. Recent results about variability are discussed in Golkhou et al. (2014, 2015). In the first paper, the authors constrained the lowest variability timescales of 938 GRBs observed until 2012 July, using the *Fermi*/Gamma Ray Burst Monitor. It has been shown that the variability timescale in the soft band (or hard X-rays observed by *Swift*) is two to three times longer than the hardest bands. Through the application of a survival analysis that take into account the upper limits and the detections, it has been discovered that less than 10% of the GRBs present variability

less than 2 ms. These particular timescales need Lorentz factors that are $\geqslant$400 as well as typical emission radii with $R \equiv 10^{14}$ cm for long GRBs and $R \equiv 3 \times 10^{13}$ cm for short GRBs. In the latter paper, using Haar wavelets, it has been established the minimum variability timescale that characterizes the light curves of GRBs. The employed approach takes the average of GRB data, determining a cumulative measure as concerns signal variation while maintaining the sensitivity for narrow pulses present in complex time series. The technique is applied to study a huge sample of the GRB light curves observed by *Swift* and given the large numbers of GRBs with known redshift it has been established for the first time the minimum rest-frame variability timescale. They discovered a minimum timescale for long-duration GRBs of 0.5 s, while the briefest timescale discovered is of 10 ms. The brief timescale implies a compact central engine. Further implications on the GRB fireball model are presented together with a correlation between the redshift and minimum timescale that may be partly caused by the redshift evolution.

LGRBs were early realized to originate from distant star-forming galaxies, and have been confidently associated with collapse of massive stars related to a supernova (SN) (Galama et al. 1998; Hjorth et al. 2003; Malesani et al. 2004; Sparre et al. 2011; Schulze et al. 2014). However, some LGRBs with no clear association with any bright SN have been discovered (Fynbo et al. 2006; Della Valle et al. 2006). This implies that there might be other progenitors for LGRBs than core-collapse SNe. Another major uncertainty concerning the progenitors of GRBs is that in the collapsar model (Woosley & Bloom 2006), LGRBs are only formed by massive stars with metallicity $Z/Z_{\odot}$ below $\simeq$0.1–0.3. On the contrary, a number of GRBs is known to be located in very metal-rich systems (Perley et al. 2015), and now one of the most important goals is to verify whether there is another way to form LGRBs besides the collapsar scenario (Greiner et al. 2015). Short GRBs, due to their small duration and energy, are consistent with a progenitor of the merger type (NS-Ns, NS-BH). The observations of the location of the short GRBs within their host galaxies tend to confirm this scenario. Additionally, this origin makes them extremely appealing as counterparts of gravitational waves (GW) as has been shown by the recently discovered GRB 170817A, where a NS-NS merger has been confirmed by the temporal coincident GW signal (Pian et al. 2017).

A common model used to explain the GRB phenomenon is the "fireball" model (Cavallo & Rees 1978) in which interactions of highly relativistic material within a jet cause the prompt phase, and interaction of the jet with the ambient material leads to the afterglow phase (Wijers et al. 1997; Mészáros et al. 1998, Mészáros 2006). In the domain of the fireball model, there are different possible mechanisms of production of the X/gamma radiation, such as the synchrotron, the Inverse Compton (IC), the blackbody radiation, and sometimes a mixture of these. There are two main flavors of the fireball: the kinetic energy dominated and the magnetic field dominated (Poynting-flux dominated).

Recently, more specific work conducted by Begue & Pe'er (2015) investigated the Poynting-flux-dominated outflow that exhibits photospheric emission. The authors demonstrate that the processes that characterize the plasma thermalization lose efficiency at a radius, which has been indicated to be beneath the photosphere radius of about two order of magnitude. A combination of the Compton scattering beneath the photosphere and the conservation of the total number of photons imposes kinetic equilibrium between photons and electrons. Consequently, this results in a rise of the photon temperature that goes up to 8 MeV, specifically when the decoupling process of the plasma occurs at the photosphere. However, the model parameters free to vary do not strongly influence the result. The researchers indicate that the expected thermal luminosity, which is a small fraction of the entire luminosity, could be observed. The magnetization of the outflows is highly constrained, as the predicted peak energy is greater than the observed peak energy that characterizes the majority of the GRBs. Continuing on this topic, Pe'er (2015) summarizes an assortment of novel ideas, new analysis methodologies, and new instruments that have revolutionized the way the prompt emission of GRBs is understood. Specifically, the author elucidates the latest observational outcomes as well as the up-to-date theoretical interpretation of the same. The time-resolved spectral analysis has been demonstrated as a huge step forward from the observational perspective. This analysis has resulted in the discovery of a distinct high-energy component that leads to the delayed observation of the GeV photons, and strong evidence regarding the presence of the thermal component in many bursts. The outcomes led to numerous theoretical efforts that were meant to highlight and comprehend the physical conditions that characterize the internal regions of the jet that emit the prompt photons and is responsible of the observed different spectral features. Key elements of Pe'er (2015)'s review are the clarification of the magnetic fields in determining the GRB spectra and their outflow, the comprehension of the microphysics involved in the magnetic and kinetic transfer of energy, particularly the process of acceleration of particles to higher energies in magnetic reconnection layers as well as shock waves, the understanding of the ways in which the dissipation of sub-photospheric energy broadens the Planck spectrum, and the geometric effects deriving from the aberration of the light.

The fireball model encounters difficulties when we aim at matching it with observations because we are not yet able to discriminate neither between the radiation mechanisms nor between these two types of fireballs. In addition, we still have to further investigate and more precisely estimate the jet opening angles and the structure of the jet itself. The crisis of the standard fireball model was reinforced when *Swift*

observations revealed a more complex behavior of the light curves (O'Brien et al. 2006; Sakamoto et al. 2007; Willingale et al. 2007; Zhang et al. 2007) than in the past, hence the discovered correlations among physical parameters are very important to discriminate between the fireball and competing theoretical models that have been presented in the literature to explain the wide variety of observations. Using these empirical relations corrected for selection biases can allow insight in the GRB emission mechanism. Moreover, the redshift range over which GRBs can be observed (up to $z = 9.4$; Cucchiara et al. 2011) is much larger than the range of the SNe Ia (up to $z = 2.26$; Rodney et al. 2015). Thus, it is extremely promising to include them as cosmological probes to understand the nature of dark energy (DE) and determine the evolution of the equation of state (EoS), $w = w(z)$, at very high z. However, GRBs cannot yet be considered standard candles because of their energies spanning eight orders of magnitude (see also Lin et al. 2015 and references therein). Therefore, finding universal relations among observable GRB properties can lead to standardize their energetics and luminosities, which is the reason why the study of GRB correlations is so crucial for understanding the GRB emission mechanism, building a reliable cosmological distance indicator, and estimating the cosmological parameters at high z. However, a big caveat needs to be considered in the evaluation of the proper cosmological parameters, as selection biases play a major and crucial role for GRBs, which are particularly affected by the Malmquist bias effect that favors the brightest objects against faint ones at large distances. Therefore, it is necessary to carefully investigate the problem of selection effects and how to overcome it before using GRB correlations as distance estimators, cosmological probes, and model discriminators; this is the main point of this review.

This review is organized as follows. In Section 2, we explain the nomenclature and definitions employed throughout this work. In Section 3, we describe how prompt correlations can be affected by selection biases. In Section 4, we present how to obtain redshift estimators, and in Section 5 we report the use of some correlations as examples of GRB applications as a cosmological tool. Finally, we provide a summary in Section 6.

2. Notations and Nomenclature

For clarity and self-completeness, we provide a brief summary of the nomenclature adopted in the review. L, F, E, S, and T indicate the luminosity, the energy flux, the energy, the fluence, and the timescale, respectively, which can be measured in several wavelengths. More specifically,

- T_{90} is the time interval in which 90% of the GRB's fluence is accumulated, starting from the time at which 5% of the total fluence was detected (Kouveliotou et al. 1993).
- $T_{\rm peak}$ is the time at which a given pulse (i.e., a sharp rise and a slower, smooth decay (Fishman et al. 1994; Norris et al. 1996; Stern & Svensson 1996; Ryde & Svensson 2002)) in the prompt light curve peaks.
- $\tau_{\rm lag}$ and $\tau_{\rm RT}$ are the difference of arrival times to the observer of the high-energy photons and low-energy photons defined between 25–50 keV and 100–300 keV energy band, and the shortest time over which the light curve increases by 50% of the peak flux of the pulse.
- T_p is the end time of the prompt phase at which the exponential decay switches to a power law, which is usually followed by a shallow decay called the plateau phase, and T_a is the time at the end of this plateau phase (Willingale et al. 2007).
- $T_{\rm break}$ is the time of a power-law break in the afterglow light curve (Sari et al. 1999; Willingale et al. 2010), i.e., the time when the afterglow brightness has a power-law decline that suddenly steepens due to the slowing down of the jet until the relativistic beaming angle roughly equals the jet opening angle $\theta_{\rm jet}$ (Rhoads 1997).
- L is the observed luminosity, and specifically $L_{\rm peak}$ and $L_{\rm iso}$ are the isotropic peak luminosity (i.e., the luminosity at the pulse peak, Norris et al. 2000) and the total isotropic mean luminosity, both in a given energy band.
- L_a, L_X are the luminosities respective to T_a, T_p.
- $E_{\rm peak}$, is the peak energy, i.e., the energy at which the νF_ν spectrum peaks.
- $E_{\rm iso}$ and E_γ the total isotropic energy emitted during the whole burst (e.g., Amati et al. 2002), the total energy corrected for the beaming factor, the latter two are connected via $E_\gamma = (1 - \cos\theta_{\rm jet})E_{\rm iso}$, respectively.
- $F_{\rm peak}$, $F_{\rm tot}$ are the peak and the total fluxes respectively (Lee & Petrosian 1996).
- S_γ and $S_{\rm obs}$ indicate the prompt fluence in the whole gamma band (i.e., from a few hundred keV to a few MeV) and the observed fluence in the range 50–300 keV.
- V is the variability of the GRB's light curve. It is computed by taking the difference between the observed light curve and its smoothed version, squaring this difference, summing these squared differences over time intervals, and appropriately normalizing the resulting sum (Reichart et al. 2001). Various smoothing filters may be applied (see also Li & Paczyński 2006 for a different approach).

Most of the quantities described above are given in the observer frame, except for $E_{\rm iso}$, $E_{\rm prompt}$, $L_{\rm peak}$ and $L_{\rm iso}$, which are already defined in the rest frame. With the upper index "$*$" we explicitly denote the observables in the GRB rest frame. The rest-frame times are the observed times divided by the cosmic time expansion, for example the rest-frame duration is denoted with $T^*_{90} = T_{90}/(1+z)$. The energetics are transformed differently, e.g., $E^*_{\rm peak} = E_{\rm peak}(1+z)$.

The Band function (Band et al. 1993) is a commonly applied phenomenological spectral profile. Its parameters are the low- and high-energy indices α and β, respectively, and the break

energy E_0. For the cases $\beta < -2$ and $\alpha > -2$, the $E_{\rm peak}$ can be derived as $E_{\rm peak} = (2 + \alpha)E_0$, which corresponds to the energy at the maximum flux in the νF_ν spectra (Band et al. 1993; Yonetoku et al. 2004).

The Pearson correlation coefficient (Kendall & Stuart 1973; Bevington & Robinson 2003) is denoted with r, the Spearman correlation coefficient (Spearman 1904) with ρ, and the p-value (a probability that a correlation is drawn by chance) is denoted with P. Finally, as most of the relations mentioned herein are power laws, we refer to their slope as to a slope of a corresponding log-log relation.

3. Selection Effects

Selection effects are distortions or biases that usually occur when the observational sample is not representative of the "true" underlying population. This kind of bias usually affects GRB correlations. Efron & Petrosian (1992), Lloyd & Petrosian (1999), Dainotti et al. (2013b), and Petrosian et al. (2013) emphasized that when dealing with a multivariate data set, it is important to focus on the intrinsic correlations between the parameters, not on the observed ones, because the latter can be just the result of selection effects due to instrumental thresholds. Moreover, how lack of knowledge about the efficiency function influences the parameters of the correlations has been already discussed for both the prompt (Butler et al. 2009) and afterglow phases (Dainotti et al. 2015b). In this Section, we revise the selection effects present in the measurements of the GRB prompt parameters described in Section 2: the peak energy, $E_{\rm peak}$, and peak luminosity, $L_{\rm peak}$, the isotropic energy, $E_{\rm iso}$, and isotropic luminosity, $L_{\rm iso}$, and the times.

3.1. Selection Effects for the Peak Energy

Mallozzi et al. (1995) discussed the photon spectra used for the determination of $E_{\rm peak}$. These parameters were obtained by averaging the count rate over the duration of each event. In addition, the temporal evolution of the single light curve affects the signal to noise ratio (S/N), i.e., a more spiky light curve will have a larger S/N than a smooth, single-peak event. However, Ford et al. (1995) showed that this effect is not relevant for $E_{\rm peak}$. Considering the most luminous GRBs, they claimed a relevant evolution of $E_{\rm peak}$ with time. For this reason, Mallozzi et al. (1995) used time-averaged spectra, resulting in an average value of $E_{\rm peak}$ for each burst. They believed that this evolution should not have a significant impact on their results. It should be noted, however, that $E_{\rm peak}$ evolution for bursts with different intensities has not yet been examined. Moreover, it has been shown that the fluence, the flux, and the peak energy are affected by data truncation caused by the detector threshold (Lee & Petrosian 1996; Lloyd & Petrosian 1999) and this will generate a bias against high $E_{\rm peak}$ bursts with small fluence or flux and an artificial positive correlation in the data. For this reason, it is important to investigate the truncation on the data before carrying out research on the correlations.

Lloyd et al. (2000) focused exemplary on the BATSE detector to understand whether truncation effects play a role in the $E_{\rm peak} - F_{\rm tot}$ correlation. As discussed in (Lloyd & Petrosian 1999), the threshold of any physical parameter determined by BATSE is obtained through the trigger condition. For each burst, $C_{\rm max}$, $C_{\rm min}$—the peak photon counts and the background in the second brightest detector—are known. Given $S_{\rm obs}$ (or $F_{\rm peak}$), the threshold can be computed using the relation

$$\frac{F_{\rm peak}}{F_{\rm peak,lim}} = \frac{S_{\rm obs}}{S_{\rm obs,lim}} = \frac{C_{\rm max}}{C_{\rm min}}. \quad (1)$$

The condition in Equation (1) is true if the GRB spectrum does not undergo severe spectral evolution. Lloyd et al. (2000) considered spectral parameters from the Band model. Given a GRB spectrum $f_{\alpha,\beta,A}(E, E_{\rm peak}, t)$, the fluence is obtained as

$$S_{\rm obs} = \int_0^T dt \int_{E_1}^{E_2} E\, f_{\alpha,\beta,A}(E, E_{\rm peak}, t) dE, \quad (2)$$

where T is the burst duration. The limiting $E_{\rm peak,lim}$, from which the BATSE instrument is still triggered, is given by the relation

$$S_{\rm obs,lim} = \int_0^T dt \int_{E_1}^{E_2} E\, f_{\alpha,\beta,A}(E, E_{\rm peak,lim}, t) dE. \quad (3)$$

To compute the lower ($E_{\rm peak,min}$) and upper ($E_{\rm peak,max}$) limits on $E_{\rm peak}$, Lloyd et al. (2000) decreased and increased, respectively, the observed value of $E_{\rm peak}$ until the condition in Equation (3) was satisfied. In addition, using non-parametric techniques developed by Efron & Petrosian (1998), they showed how to correctly remove selection bias from observed correlations. This method is general for any kind of correlation. Next, similar to what was done by Lloyd & Petrosian (1999), once $E_{\rm peak,min}$ and $E_{\rm peak,max}$ were determined, Lloyd et al. (2000) showed that the intrinsic $E_{\rm peak}$ distribution is much broader than the observed one. Therefore, they analyzed how these biases influence the outcomes. After a careful study of the selection effects, it was claimed that an intrinsic correlation between $E_{\rm peak}$ and $E_{\rm iso}$ indeed exists. In addition, as an important constraint on physical models of GRB prompt emission, the $E_{\rm peak}$ distribution is broader than that inferred previously from the observed $E_{\rm peak}$ values of bright BATSE GRBs (Zhang & Mészáros 2002).

The $E_{\rm peak}$ and $E_{\rm iso}$ correlation, a.k.a. "the Amati relation", was actually discovered in 2002 (Amati et al. 2002) based on the first sample of *BeppoSAX* GRBs with measured redshift, and later confirmed and extended by measurements by *HETE-2*, *Swift*, *Fermi*/GBM, Konus–WIND (Figure 1, left panel). The fact that detectors with different sensitivities as a function of photon energy observe a similar correlation is a first–order indication that instrumental effects should not be dominant. Soon after, it was shown that the same correlation holds

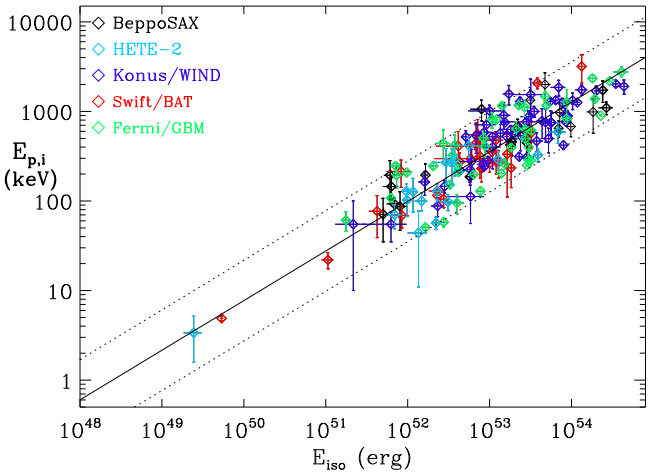

Figure 1. Left: the $E_{\rm peak} - E_{\rm iso}$ correlation in long GRBs as shown in Amati & Della Valle (2013).

between $E_{\rm peak}$ and the peak luminosity $L_{\rm peak}$ (Yonetoku et al. 2004). Moreover, it was pointed out by Ghirlanda et al. (2004) that the $E_{\rm peak}$ and $E_{\rm iso}$ correlation becomes tighter and steeper ("the Ghirlanda relation") when applying the correction for the jet opening angle. This correction, however, can be applied only for the subsample of GRBs from which this quantity could be estimated based on the break observed in the afterglow light curve. In addition, this method of estimating the jet opening angle is model dependent and may be affected by uncertainties.

Later, Band & Preece (2005) showed that the Amati and the Ghirlanda relation could be converted into a similar energy ratio

$$\frac{E_{\rm peak}^{1/\eta_i}}{S_\gamma} \propto F(z). \tag{4}$$

Here, η_i are the best-fit power-law indices for the respective correlations. These energy ratios can be represented as functions of redshift, $F(z)$, and their upper limits could be determined for any z. The upper limits of the energy ratio of both the Amati and Ghirlanda relations can be projected onto the peak energy-fluence plane where they become lower limits. In this way, it is possible to use GRBs without redshift measurement to test the correlations of the intrinsic peak energy $E_{\rm peak}$ with the radiated energy ($E_{\rm iso}$, E_γ) or peak luminosity ($L_{\rm peak}$), as shown in Figure 2. By using this method the above and other authors (Goldstein et al. 2010; Collazzi et al. 2012) found that a significant fraction of BATSE and Fermi GRBs are potentially inconsistent with the $E_{\rm peak}$ and $E_{\rm iso}$ correlation.

However, several other authors (Bosnjak et al. 2008; Ghirlanda et al. 2008; Nava et al. 2012) showed that, when properly taking into account the dispersion of the correlation and the uncertainties on spectral parameters and fluencies, only a few percent of GRBs may be outliers of the correlation. Moreover, it can be demonstrated (Dichiara et al. 2013) that such a small fraction of outliers can be artificially created by the combination of instrumental sensitivity and energy band, namely the typical hard–to–soft spectral evolution of GRBs.

Along this line of investigations, recently, Bošnjak et al. (2014) presented the evaluation of $E_{\rm peak}$ based on the updated *INTEGRAL* catalog of GRBs observed between 2002 December and 2012 February. In their spectral analysis they investigated the energy regions with highest sensitivity to compute the spectral peak energies. To account for the possible biases in the distribution of the spectral parameters, they compared the GRBs detected by *INTEGRAL* with the ones observed by *Fermi* and BATSE within the same fluence range. A lower flux limit ($<8.7 \times 10^{-5}$ erg cm^{-2} in 50–300 keV energy range) was assumed because the peak fluxes from different telescopes were computed in distinct energy ranges. Then, with the proper evaluation of $E_{\rm peak}$, they considered correlations between the following parameters: i) $E_{\rm peak}$ and $F_{\rm tot}$, ii) $E_{\rm peak}$ and α, and iii) $E0$ and α.

In case of the $E_{\rm peak} - \alpha$ relation no significant correlation was found, while for the $E_0 - \alpha$ relation there was a weak negative correlation ($\rho = -0.44$) with $P = 1.15 \times 10^{-2}$. In case of the $E_{\rm peak} - F_{\rm tot}$ relation, a weak positive correlation ($\rho = 0.50$) was found with $P = 1.88 \times 10^{-2}$. This is in agreement with the results of Kaneko et al. (2006), who found a significant correlation between $E_{\rm peak}$ and $F_{\rm tot}$ analyzing the spectra of 350 bright BATSE GRBs with high spectral and temporal resolution. Regarding the detector-related $E_{\rm peak}$ uncertainties, Collazzi et al. (2011) noticed that there is a discrepancy among the values of $E_{\rm peak}$ found in literature that go beyond the 1σ uncertainty.

Finally, notwithstanding that GRBs must be sufficiently bright to perform a time-resolved spectroscopy and have known redshifts, if the process generating GRBs is independent of the brightness then the existence of the time-resolved $E_{\rm peak} - L_{\rm iso}$ correlation (Ghirlanda et al. 2010; Lu et al. 2012; Frontera et al. 2012), see Figure 1 right panel, is a further evidence that these $E_{\rm peak}$—"intensity" correlations have a physical origin linked to the main emission mechanism in GRBs.

3.2. Selection Effects for the Isotropic Energy

Regarding the selection effects related to $E_{\rm iso}$, Amati et al. (2002) found that the GRBs with measured redshift can be biased due to their paucity, and that the sensitivities and energy bands of the Wide Field Camera (WFC) and Gamma-ray Burst Monitor (GBM) onboard *BeppoSAX* and *Fermi*, respectively, might prefer energetic and luminous GRBs at larger redshifts, thus creating an artificial $E_{\rm peak} - E_{\rm iso}$ relation.

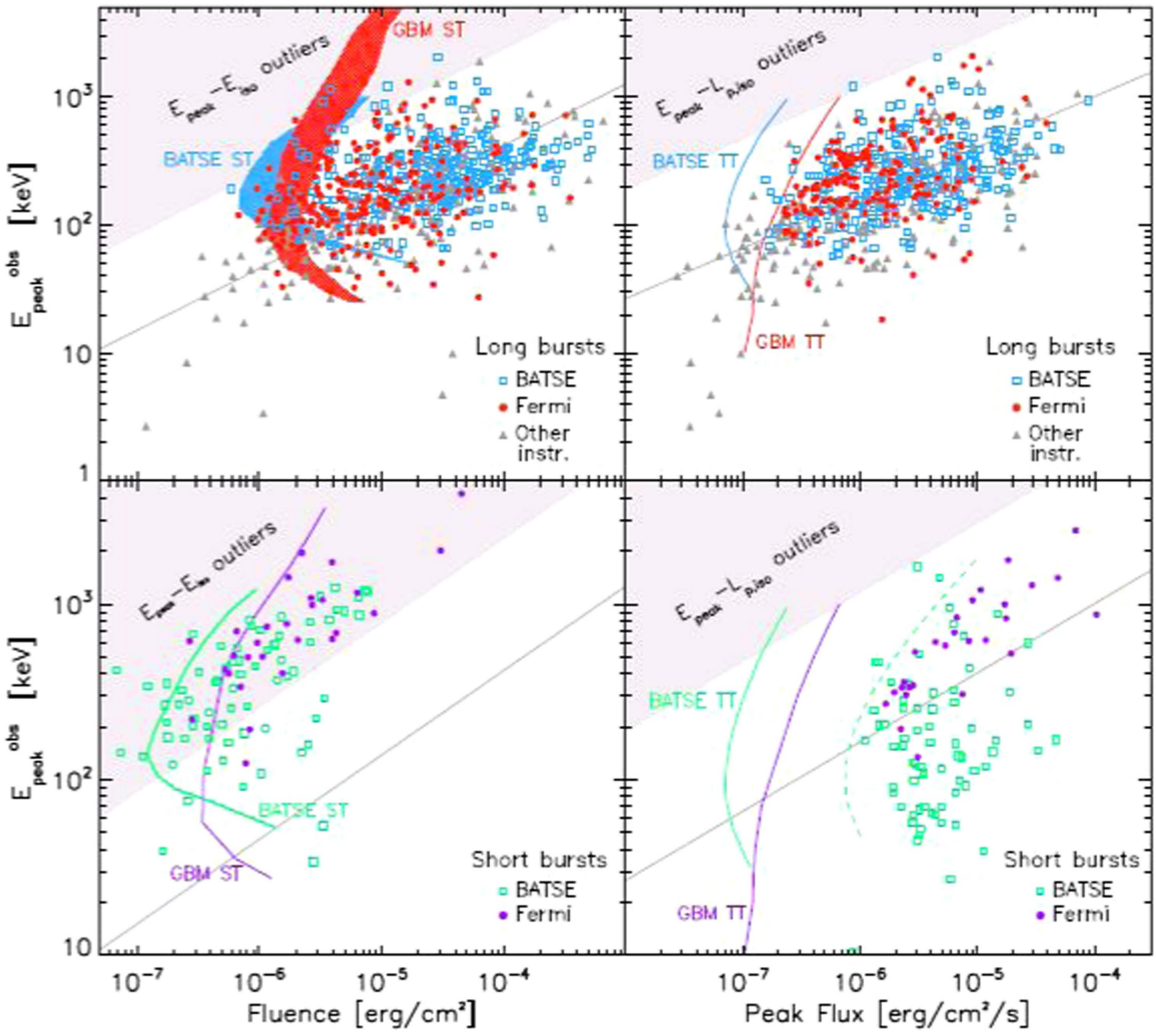

Figure 2. $E_{\rm peak}$—fluence and $E_{\rm peak}$—peak flux planes for long (upper panels) and short (bottom panels) bursts (Nava et al. 2012). Empty squares represent BATSE bursts, filled circles represent GBM bursts and filled triangles indicate events detected by other instruments. In all panels the instrumental limits for BATSE and GMB are reported: shaded curved regions in the upper-left panel show the fluence threshold, estimated assuming burst duration of 5 and 20 s; solid curves in the bottom-left panel represent the fluence threshold for short bursts. Solid curves in the right-hand panels define the trigger threshold, identical for short and long events. The dashed curve in the bottom-right panel represents the selection criterion applied, i.e., Peak flux $\geqslant$3 photons cm^{-2} s^{-1}. The shaded regions in the upper-left corners of all the planes are the region identifying the outliers at more than 3σ of the $E_{\rm peak} - E_{\rm iso}$ (left-hand panels) and $E_{\rm peak} - L_{\rm peak}$ (right-hand panels) correlations for any given redshift. GRBs, without measured redshift, which fall in these regions are outliers of the corresponding rest-frame correlations ($E_{\rm peak} - E_{\rm iso}$ and $E_{\rm peak} - L_{\rm peak}$ for the left- and right-hand panels, respectively) for any assigned redshift. It means that there is no redshift which makes them consistent with these correlations (considering their 3σ scatter).

Therefore, similarly to Lloyd & Petrosian (1999) as discussed in Section 3.1, Amati et al. (2002) analyzed the $E_{\rm peak,min}$ and $E_{\rm peak,max}$ for which the $E_{\rm peak} - E_{\rm iso}$ correlation exists. If the spectral parameters are coincident with their minimum and maximum values then it is very likely that data truncation will produce a spurious correlation.

Considering a sample of BATSE GRBs without measured redshifts, two research groups (Nakar & Piran 2005; Band & Preece 2005) claimed that around 50% (Nakar & Piran 2005) or even 80% (Band & Preece 2005) of GRBs do not obey the $E_{\rm peak} - E_{\rm iso}$ correlation. This is due to the fact that the selection effects may favor a burst sub-population for which the Amati relation is valid. GRBs with determined redshifts must be relatively bright and soft to be localized. In addition, it was found that selection effects were present in these GRB observations and this is the reason why only the redshifts of the GRBs obeying the relation were computed. However, other authors (Ghirlanda et al. 2005; Bosnjak et al. 2008) arrived at opposite conclusions and these different results are due to considering (or not) the dispersion in the relation, and the

uncertainties in $E_{\rm peak}$ and the fluence. Indeed, considering both these features, only some BATSE GRBs with no measured redshift may be considered outliers of the $E_{\rm peak} - E_{\rm iso}$ relation (Ghirlanda et al. 2005).

Later, Amati (2006) overestimated $E_{\rm peak}$ values because of the paucity of data below 25 keV. Indeed, if there were selection effects in the sample of *HETE-2* GRBs with known redshift, they were more plausible to occur due to detector sensitivity as a function of energy than as a function of the redshift (Amati 2006). The fact that all *Swift* GRBs with known redshift are consistent with the $E_{\rm peak} - E_{\rm iso}$ correlation is a strong evidence against the existence of relevant selection effects. Amati (2006) justified this statement adducing the following points: i) the *Swift*/BAT sensitivity in 15–30 keV is comparable with that of BATSE, BeppoSAX and *HETE-2*, ii) the rapid XRT localization of GRBs decreased the selection effects dependent on the redshift estimate. However, BAT gives an estimate of $E_{\rm peak}$ only for 15%–20% of the events. Besides, it was also claimed that the existence of sub-energetic events (like GRB 980425 and possibly GRB 031203) with spectral characteristics are not in agreement with the obtained relation.

Ghirlanda et al. (2008) studied the redshift evolution of the $E_{\rm peak} - E_{\rm iso}$ correlation by binning the GRB sample into different redshift ranges and comparing the slopes in each bin. There is no evidence that this relation evolves with z, contrary to what was found with a smaller GRB sample. Their analysis showed, however, that the bursts detected before *Swift* are not influenced by the instrumental selection effects, while in the sample of *Swift* GRBs the smallest fluence for which it is allowed to compute $E_{\rm peak}$ suffers from truncation effects in 27 out of 76 events.

Amati et al. (2009) analyzed the scatter of the $E_{\rm peak} - E_{\rm iso}$ relation at high energies and pointed out that it is not influenced by truncation effects because its normalization, computed assuming GRBs with precise $E_{\rm peak}$ from *Fermi*/GBM, is in agreement with those calculated from other satellites (e.g., *BeppoSAX*, *Swift*, *KONUS*/Wind). It was also checked whether $E_{\rm iso}$ in the 1 keV–10 MeV band can affect the $E_{\rm peak} - E_{\rm iso}$ relation, but its scatter does not seem to vary. Finally, it was also pointed out that: i) the distribution of the new sample of 95 LGRBs is consistent with previous results, ii) in the $E_{\rm peak} - E_{\rm iso}$ plane the scatter is smaller than in the $E_{\rm peak} - F_{\rm tot}$ plane, but if the redshift is randomly distributed then the distributions are similar, and iii) all LGRBs with measured redshift (except GRB 980425) detected with *Fermi*/GBM, *BeppoSAX*, *HETE-2*, and *Swift*, obey the $E_{\rm peak} - E_{\rm iso}$ relation (Amati et al. 2008). An exhaustive analysis of instrumental and selection effects for the $E_{\rm peak} - E_{\rm iso}$ correlation is underway and will be reported elsewhere.

Another example of an analysis of selection effects for $E_{\rm iso}$ was given by Butler et al. (2009). They studied the influence of the detector threshold on the $E_{\rm peak} - E_{\rm iso}$ relation, considering a set of 218 *Swift* GRBs and 56 *HETE-2* ones. Due to the different sensitivities of *Swift* and *HETE-2* instruments, in the *Swift* survey more GRBs are detected. In other words, there is a deficit of data in samples observed in the pre-*Swift* missions, and this possibly biases the correlations. Butler et al. (2009) tested the reliability of a generic method for dealing with data truncation in the correlations, and afterwards they employed it to data sets obtained by *Swift* and pre-*Swift* satellites. However, *Swift* data does not rigorously satisfy the independence from redshift if there are only bright GRBs, as instead occurred for the pre-*Swift* $E_{\rm peak} - E_{\rm iso}$ relation.

Later, Collazzi et al. (2012) argued that the Amati relation may be an artifact of, or at least significantly biased by, a combination of selection effects due to detector sensitivity and energy thresholds. It was found that GRBs following the Amati relation are distributed above a limiting line. Even if bursts with spectroscopic redshifts are consistent with Amati's limit, it is not true for bursts with spectroscopic redshift measured by BATSE and *Swift*. In the case in which selection effects are significant, the data in an $E_{\rm peak} - E_{\rm iso}$ plane, obtained by distinct satellites, display different distributions. Eventually, it was pointed out that the selection effects for a detector with a high threshold allow detecting only GRBs in the area where GRBs follow the Amati relation (the so-called Amati region), hence these GRBs are not useful cosmological probes.

Continuing on investigating the reliability of the Amati relation, Kocevski (2012) reproduced this relation via a population synthesis code, which is used to mimic the prompt emission of GRBs. Under given assumptions on the distributions of spectral parameters and the luminosity function of the population as well as the comoving rate density, the author investigates how bursts of disparate spectral features, as well as redshift, would seem to a gamma-ray detector on earth in the observer frame. It is discovered that the Amati correlation can be reproduced, despite the initial simulations would barely assume a weak association among the $E_{\rm peak}$ and $E_{\rm iso}$ variables. Thus, the left boundary of the correlation for the low luminous GRBs would have been produced by the limited flux detection threshold. Contrariwise, due to the Malmquist bias effects only the brightest GRBs are observed at large redshifts, leading to the problem of having undetected bursts of high $E_{\rm iso}$ and low $E_{\rm peak}$, since the redshifted $E_{\rm peak}$ would undergo to energies whereby the detectors lose their sensitivity. For this reason, this correlation could be due to several concomitant factors, the detection threshold of the instrument, the intrinsic limit in the GRB luminosity function, and the extensive redshift. Although in this treatment the model used is simplified, it is crucial to understand that selection effects can bias and undermine the reliability of observed correlations.

Instead, the main conclusion drawn from the research of Heussaff et al. (2013) is that the $E_{\rm peak} - E_{\rm iso}$ relation is generated by a physical constraint that does not allow the existence of high values of $E_{\rm iso}$ and low values of $E_{\rm peak}$, and

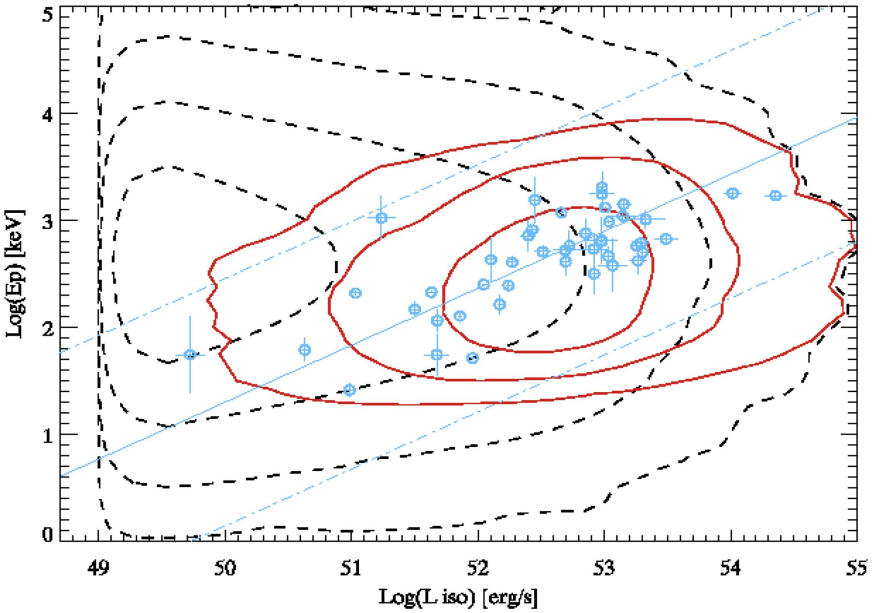

Figure 3. Simulation showing the variation of the density from (Ghirlanda et al. 2012). The simulated sample is represented by the dashed contour (1, 2, 3, and 4σ levels). The sample of simulated GRBs with a flux greater than the constraint $F_{\rm lim} = 2.6$ ph cm^{-2} s^{-1} in the 15–150 keV energy band is depicted by red solid contours (1, 2, and 3σ levels). The blue circles denote the 46 *Swift* GRBs used by Nava et al. (2012): the solid line represents the best fit of the $L_{\rm iso} - E_{\rm peak}$ relation, and the dot-dashed lines display the 3σ region around the best-fit line.

that the sensitivity of γ-ray and optical detectors favors GRBs located in the $E_{\rm peak} - E_{\rm iso}$ plane near these constraints. These two effects seem to explain the different results obtained by several authors investigating the $E_{\rm peak} - E_{\rm iso}$ relation.

Amati & Della Valle (2013), to further discuss the issue of the dependence of the Amati relation on the redshift, analyzed the reliability of the $E_{\rm peak} - E_{\rm iso}$ relation using a sample of 156 GRBs available until the end of 2012. They divided this sample into subsets with different redshift ranges (e.g., $0.1 < z < 1$, $1 < z < 2$, etc.), pointing out that the selection effects are not significant because the slope, normalization, and scatter of the correlation remain constant. They found

$$\log \frac{E_{\rm peak}}{1\ {\rm keV}} = 0.5 \log \frac{E_{\rm iso}}{10^{52}\ {\rm erg}} + 2. \quad (5)$$

Finally, Mochkovitch & Nava (2015), with a model that took into account the small amount of GRBs with large $E_{\rm iso}$ and small $E_{\rm peak}$, pointed out that the scatter of the intrinsic $E_{\rm peak} - E_{\rm iso}$ relation is larger than the scatter of the observed one.

3.3. Selection Effects for the Isotropic Luminosity

Ghirlanda et al. (2012) studied a data set of 46 GRBs and claimed that the flux limit—introduced to take into account selection biases related to $L_{\rm iso}$—generates a constraint in the $L_{\rm iso} - E_{\rm peak}$ plane. Given that this constraint corresponds to the observed relation, they pointed out that 87% of the simulations gave a statistically meaningful correlation, but only 12% returned the slope, normalization, and scatter compatible with those of the original data set. There is a non-negligible chance that a boundary with asymmetric scatter may exist due to some intrinsic features of GRBs, but to validate this hypothesis additional complex simulations would be required.

Additionally, they performed Monte Carlo simulations of the GRB population under different assumptions for their luminosity functions. Assuming there is no correlation between $E_{\rm peak}$ and $L_{\rm iso}$, they were unable to reproduce it, thus confirming the existence of an intrinsic correlation between $E_{\rm peak}$ and $L_{\rm iso}$ at more than 2.7σ. For this reason, there should be a relation between these two parameters that does not originate from detector limits (see Figure 3).

3.4. Selection Effects for the Peak Luminosity

Yonetoku et al. (2010) investigated how the truncation effects and the redshift evolution affect the $L_{\rm peak} - E_{\rm peak}$ relation. They claimed that the selection bias due to truncations might occur when the detected signal is comparable with the detector threshold, and showed that the relation is indeed redshift-dependent.

Shahmoradi et al. (2013) studied the $E_{\rm peak} - E_{\rm iso}$ and $L_{\rm peak} - E_{\rm peak}$ relations, and constructed a model describing both the luminosity function and the distribution of the prompt spectral and temporal parameters, taking into account the detection threshold of γ-ray instruments, particularly BATSE

and *Fermi*/GBM. Analyzing the prompt emission data of 2130 BATSE GRBs, he demonstrated that SGRBs and LGRBs are similar in a 4-dimensional space of $L_{\rm peak}$, $E_{\rm iso}$, $E_{\rm peak}$ and T_{90}. Moreover, he showed that these two relations are strongly biased by selection effects, questioning their usefulness as cosmological probes. Similar $E_{\rm peak} - E_{\rm iso}$ and $L_{\rm peak} - E_{\rm peak}$ relations, with analogous correlation coefficient and significance, should hold for SGRBs. Based on the multivariate log-normal distribution used to model the luminosity function it was predicted that the strong correlation between $T90$ and both $E_{\rm iso}$ and $L_{\rm peak}$ was valid for SGRBs as well as for LGRBs.

Shahmoradi & Nemiroff (2015) investigated the luminosity function, energetics, relations among GRB prompt parameters, and methodology for classifying SGRBs and LGRBs using 1931 BATSE events. Employing again the multivariate log-normal distribution model, they found out statistically meaningful $L_{\rm peak} - E_{\rm peak}$ and $E_{\rm peak} - E_{\rm iso}$ relations with $\rho = 0.51 \pm 0.10$ and $\rho = 0.60 \pm 0.06$, respectively.

Yonetoku et al. (2004), Petrosian et al. (2015) showed how $L_{\rm peak}$ undergoes redshift evolution. These authors found a strong redshift evolution, $L_{\rm peak} \propto (1+z)^{2.0-2.3}$, an evolution which is roughly compatible in 1.5σ among the authors. Different data samples were used, but statistical method, i.e., the Efron & Petrosian (1992) one, was the same. This tool uses a non-parametric approach, a modification of the Kendall τ statistics. A simple $[f(z) = (1+z)^{\alpha}]$ or a more complex redshift function was chosen and in both cases compatible results were found for the evolution. After a proper correction of the $L_{\rm peak}$ evolution, Dainotti et al. (2015a) established the intrinsic $L_{\rm peak} - L_X$ relation. This statistical method is very general and it can be applied also to properties of the afterglow emission. For example, Dainotti et al. (2013b) found the evolution functions for the luminosity at the end of the plateau emission, L_X, and its rest-frame duration, T_a^*, a.k.a the Dainotti relation, and they demonstrated the intrinsic nature of the $L_X - T_a^*$ relation. From the existence of the intrinsic nature of $L_X - T_a^*$ and $L_{\rm peak} - L_X$ relations Dainotti et al. (2016) discovered the extended $L_X - T_a^* - L_{\rm peak}$ relation, which is intrinsic as being a combination of two intrinsic correlations. However, in this paper the authors had to deal with additional selection bias problems. They analyzed two samples, the full set of 122 GRBs and the gold sample composed of 40 GRBs with high quality data in the plateau emission. The selection criteria were defined carefully enough not to introduce any biases, which were shown to be indeed valid by a statistical comparison of the whole and gold sample. They found a tight $L_a - T_a^* - L_{\rm peak}$ relation, and showed that for the gold sample it has a 54% smaller scatter than a corresponding $L_a - T_a^*$ relation obtained for the whole sample. Moreover, it was shown via the bootstrapping method that the reduction of scatter is not due to the smaller sample size, hence the 3D relation for the gold sample is intrinsic in nature, and is not biased by the selection effects of this sample. It follows that a more careful consideration of the selection effects can provide insight into the physics underlying the GRB emission mechanism. In fact, this fundamental plane relation can be a very reliable test for physical models. An open question would be if the magnetar model (Zhang & Mészáros 2001; Troja et al. 2007; Rowlinson et al. 2014; Rea et al. 2015) can still be a plausible explanation of this relation as it was for the $L_X - T_a^*$ relation. Thus, once correlations are corrected for selection bias can be very good candidates to test and possibly efficiently discriminate among plausible theoretical models.

3.5. Selection Effects for the Lag Time and the Rise Time

Considering $\tau_{\rm lag}$ and its dependence on the redshift, Azzam (2012) studied the evolutionary effects of the $L_{\rm peak} - \tau_{\rm lag}$ relation using 19 GRBs detected by *Swift*, and found the results to be in perfect agreement with those obtained through other methods (like the ones from Tsutsui et al. 2008, who used redshifts obtained through the Yonetoku relation to study the dependence of the $L_{\rm peak} - \tau_{\rm lag}$ one on redshift). Specifically, he divided the data sample in 3 redshift ranges (i.e., 0.540–1.091, 1.101–1.727, 1.949–3.913) and calculated the slope and normalization of the log-log relation in each of them. In the first bin a slope of -0.92 ± 0.19 and a normalization of 51.94 ± 0.11 were found with $r = -0.89$. In the second bin the slope was -0.82 ± 0.12 and the normalization 52.12 ± 0.08 with $r = -0.94$. In the third bin the relation had a slope equal to -0.04 ± 0.22 and normalization 52.90 ± 0.12 with $r = -0.06$. Therefore, the $L_{\rm peak} - \tau_{\rm lag}$ relation seems to evolve with redshift, however, this conclusion is only tentative since there is the problem that each redshift range is not equally populated, and it is limited by low statistics and by the significant scatter in the relation. Therefore, the $L_{\rm peak} - \tau_{\rm lag}$ relation is redshift-dependent, but this result is not conclusive due to the paucity of the sample and a significant scatter.

Kocevski & Petrosian (2013) found that in individual pulses the observer-frame cosmological time dilation is masked out because only the most luminous part of the light curve can be observed by GRB detectors. Therefore, the duration and $E_{\rm iso}$ for GRBs close to the detector threshold need to be considered as lower limits, and the temporal characteristics are not sufficient to discriminate between LGRBs and SGRBs (see also Tarnopolski 2015b for a novel and successful attempt of using for this purpose non-standard parameters via machine learning).

Regarding instead the rise time, Wang et al. (2011) used 72 LGRBs observed by *BeppoSAX* and *Swift* to study the $L_{\rm iso} - \tau_{\rm RT}$ relation, and found that the relation is not dependent

on the redshift. In fact, for the total sample they obtained

$$\log \frac{L_{\rm iso}}{1 {\rm erg\ s^{-1}}} = (52.68 \pm 0.07) - (1.12 \pm 0.14) \log \frac{\tau^*_{\rm RT}}{0.1\ {\rm s}}, \quad (6)$$

with $\sigma_{\rm int} = 0.48 \pm 0.05$. Additionally, dividing the data set into four redshift bins (i.e., 0–1, 1–2, 2–3, and 3–8.5), the slope and normalization of this relation remained nearly constant. This represents good evidence for the $L_{\rm iso} - \tau_{\rm RT}$ relation not being influenced by evolutionary effects.

4. Redshift Estimators

As we have already pointed out, it is relevant to study GRBs as possible distance estimators, since for many of them z is unknown. Therefore, having a relation which is able to infer the distance from observed quantities independent on z would allow a better investigation of the GRB population. Moreover, in the cases in which z is uncertain, its estimators can give hints on the upper and lower limits of the GRB's distance. Some examples of redshift estimators from the prompt relations (Atteia 2003; Yonetoku et al. 2004; Tsutsui et al. 2013) have been reported.

In (Atteia 2003), the $E_{\rm peak} - E_{\rm iso}$ relation, due to the dependence of these quantities on $D_L(z, \Omega_M, \Omega_\Lambda)$, was analyzed to derive pseudo-redshifts of 17 GRBs detected by *BeppoSAX*. They were obtained in the following way: in a first step a combination of physical parameters was considered: $X = \frac{n_\gamma \sqrt{T_{90}}}{E_{\rm peak}}$, where n_γ is the observed number of photons, and then the theoretical evolution of this parameter with z was computed according to

$$X = A f(z), \quad (7)$$

where A is a constant and $f(z)$ is the redshift evolution for the energy spectra of a "standard" GRB. A "standard" GRB has $\alpha = -1.0$, $\beta = -2.3$, and $E_0 = 250$ keV in a ΛCDM universe ($H_0 = 65$ km s^{-1} Mpc^{-1}, $\Omega_M = 0.3$, $\Omega_\Lambda = 0.7$). The relation representing the redshift evolution was inverted to derive a redshift estimator from the observed quantities given by the equation $z = \frac{1}{A} f^{-1}(X)$. The possible applications of these redshift estimators include a statistically-driven method to compare the distance distributions of different GRB populations, a rapid identification of faraway GRBs with redshifts exceeding three, and estimates of the high-z star formation rate.

Yonetoku et al. (2004), using 689 bright BATSE LGRBs, analyzed the spectra of GRBs adopting the Band model. The lower flux limit was set to $F_{\rm lim} = 2 \times 10^{-7}$ erg cm^{-2} s^{-1} for achieving a higher S/N ratio. Next, $F_{\rm peak}$ and $E^*_{\rm peak}$ were obtained and the pseudo-redshifts of GRBs in the sample were estimated inverting with respect to z the following equation

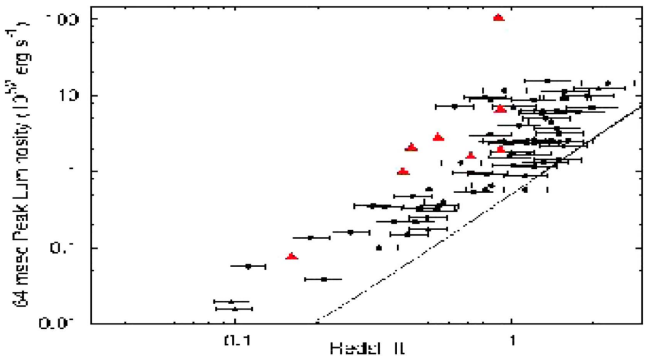

Figure 4. Distribution of z estimated by the best-fit $\log L_{\rm peak} - \log E_{\rm peak}$ relation for SGRBs from (Tsutsui et al. 2013); 71 bright BATSE SGRBs from (Ghirlanda et al. 2009) were used. Black dots denote the pseudo-redshifts related to $L_{\rm peak}$, and red filled triangles mark secure SGRBs; $z \in (0.097, 2.581)$ with $\langle z \rangle = 1.05$, compared with *Swift* LGRBs with $\langle z \rangle \approx 2.16$. The solid line represents the flux limit of $F_{\rm peak} = 10^{-6}$ erg cm^{-2} s^{-1}.

(taking into account the redshift dependence on $D_L(z, \Omega_M, \Omega_\Lambda)$):

$$\log L_{\rm peak} = (47.37 \pm 0.37) + (2.0 \pm 0.2) \log E^*_{\rm peak}. \quad (8)$$

Later, in (Tsutsui et al. 2013) the $E_{\rm peak} - E_{\rm iso}$ and the $L_{\rm peak} - E_{\rm peak}$ relations were tested using a sample of 71 SGRBs detected by BATSE. Comparing these two relations, it was claimed that the $L_{\rm peak} - E_{\rm peak}$ one would be a better redshift estimator because it is tighter. Therefore, rewriting the $L_{\rm peak} - E_{\rm peak}$ relation in the following way:

$$\frac{D_L^2(z, \Omega_M, \Omega_\Lambda)}{(1+z)^{1.59}} = \frac{10^{52.29}}{4\pi F_{\rm peak}} \left(\frac{E_{\rm peak}}{774.5} \right)^{1.59}, \quad (9)$$

and assuming a cosmological model with $(\Omega_M, \Omega_\Lambda) = (0.3, 0.7)$, the pseudo-redshifts were calculated from $D_L(z, \Omega_M, \Omega_\Lambda)$, which is a function of z (see Figure 4). Dainotti et al. (2011) investigated the possibility of using the $L_X - T^*_a$ relation as a redshift estimator. It appeared that only if one is able to reduce the scatter of the relation to 20% and be able to select only GRBs with low error bars in their variables, satisfactory results can be achieved. More encouraging results for the redshift estimator are expected with the use of the new 3D (Dainotti et al. 2016b) correlation due to its reduced scatter.

Burgess et al. (2015) studied the hardness-intensity correlation, also named the Golenetskii correlation, between the spectral peak energy inside a burst and its instantaneous luminosity to assess its use as possible redshift estimator. To this end, the author used the hierarchical Bayesian model to examine if this correlation can be used as redshift estimator. By applying the correlations power law, the indices of the law gather around a common value, yet with a variance broader than the ones initially computed. Also, the intrinsic rest-frame normalization of the correlation had 10^{51}–10^{53} erg s^1 as a spread. This implies that there are disparate physical setups concerning the emission such as magnetic field strength,

number of emitting electrons, photospheric radius, viewing angle, etc. Consequently, the hardness-intensity correlation is not an effective tool for the determination of the redshift. However, the Bayesian approach in the present study permits an effective determination of the correlation properties in the rest frame, and thus allows establishing additional constraints for the emissions physical models.

The possibility of using a GRB prompt emission relation, a modified version of the so-called Yonetoku relation (Yonetoku et al. 2004), to derive the redshift has been discussed by Guiriec et al. (2013, 2016a, 2016b). For discussion about this relation between the luminosity of the non-thermal component, LinTh, and its corresponding spectral peak energy in the rest frame, $E_{peak,iNT}$ within the context of the other prompt relations see Dainotti et al. (2018). The relation led to an estimate of a few redshifts.

Another problem that rises from the investigation of the relation is the computation of the intrinsic scatter. In Andreon (2013) this issue is examined together with the problematic aspects that characterize the astronomical data including upper/lower limits, selection effects (also due to data collection), intrinsic scatter, populations biased from the Malmquist selection effect, non-Gaussian data etc. The author indicates the way it is possible modeling the features of the data through the Bayesian methods. In summary, the posterior probability distribution give information about the knowledge we have on the examined quantities after the data has been analyzed and when Monte Carlo programs are used for the computation. This work is relevant because indicates how to constrain for example the cosmological parameters derived from SNe data as well as to validate the fitting model and present their respective coding.

5. Cosmology

The Hubble Diagram (HD) of SNe Ia, i.e the distribution of the distance modulus[4] $\mu(z)$, opened the way to the investigation of the nature of DE. As is well known, $\mu(z)$ scales linearly with the logarithm of the luminosity distance $D_L(z, \Omega_M, \Omega_\Lambda)$ (which depends on the DE EoS through a double integration) as follows:

$$\mu(z) = 25 + 5 \log D_L(z, \Omega_M, \Omega_\Lambda). \quad (10)$$

Discriminating among different models requires extending the HD to higher redshifts since the expression for $\mu(z)$ is different as one goes to higher z values.

5.1. The Problem of the Calibration

One of the most important issues presented in the use of GRB correlations for cosmological studies is the so-called circularity problem. Since local GRBs, i.e., GRBs with $z \leqslant 0.01$, are not available, an exception being GRB 980425 with $z = 0.0085$ (Galama et al. 1998), one has to typically assume an a priori cosmological model to compute $D_L(z, \Omega_M, \Omega_\Lambda)$ so that the calibration of the two dimensional (2D) correlations turns out to be model dependent. In principle, such a problem could be avoided in three ways. First, through the calibration of these correlations by several low-z GRBs (in fact, at $z \leqslant 0.1$ the luminosity distance has a negligible dependence on the choice of cosmological parameters). Second, a solid theoretical model has to be found to physically motivate the observed 2D correlations, thus setting their calibration parameters. Particularly this would fix their slopes independently of cosmology, but this task still has to be achieved.

Another option for calibrating GRBs as standard candles is to perform the fitting using GRBs with z in a narrow range, Δz, around some representative redshift, z_c. We here describe some examples on how to overcome the problem of circularity using prompt correlations. GRB luminosity indicators were generally written in the form of $L = a \prod x_i^{b_i}$, where a is the normalization, x_i is the i-th observable, and b_i is its corresponding power-law index. However, Liang & Zhang (2006) employed a new GRB luminosity indicator, $E_{\rm iso} = aE_{\rm peak}^{*b_1} T_{\rm peak}^{*b_2}$ (the LZ relation, Liang & Zhang 2005), and showed that while the dependence of a on the cosmological parameters is strong, it is weak for $b1$ and b_2 as long as Δz is sufficiently small. The selection of Δz is based on the size and the observational uncertainty of a particular sample. Liang & Zhang (2005) proposed to perform the calibration on GRBs with z clustered around an intermediate $z_c \in (1, 2.5)$, because most GRBs are observed with such redshifts. Eventually, it was found that ~25 GRBs around $z_c = 1$ with $\Delta z = 0.3$ is sufficient for the calibration of the LZ relation to serve as a distance indicator.

Also Ghirlanda et al. (2006), using the $E_{\rm peak} - E_\gamma$ correlation (Ghirlanda et al. 2004) defined $E_{\rm peak} = aE_\gamma^b$ as a luminosity indicator. Considering a sample of 19 GRBs detected by *BeppoSAX* and *Swift*, the minimum number of GRBs required for calibration of the correlation, N, was estimated within a range Δz centered around a certain z_c. For a set of Ω_M and Ω_Λ the correlation was fitted using a sample of N GRBs simulated in the interval $(z_c - \Delta z, z_c + \Delta z)$. The relation was considered to be calibrated if the change of the exponent b was smaller than 1%. The free parameters of this test are N, Δz and z_c. Different values of z_c and $\Delta z \in (0.05, 0.5)$ were tested by means of a Monte Carlo technique. At any z the smaller the N, the larger was the variation Δb of the exponent (for the same Δz) due to the correlation being less constrained. Instead, for larger z_c, smaller Δz was sufficient for maintaining Δb small. It was found that only 12 GRBs within $z \in (0.9, 1.1)$ are enough to calibrate the $E_{\rm peak} - E_\gamma$ relation.

Unfortunately, this method might not be working properly due to the paucity of the observed GRBs. Another method to

[4] The difference between the apparent magnitude m, ideally corrected from the effects of interstellar absorption, and the absolute magnitude M of an astronomical object.

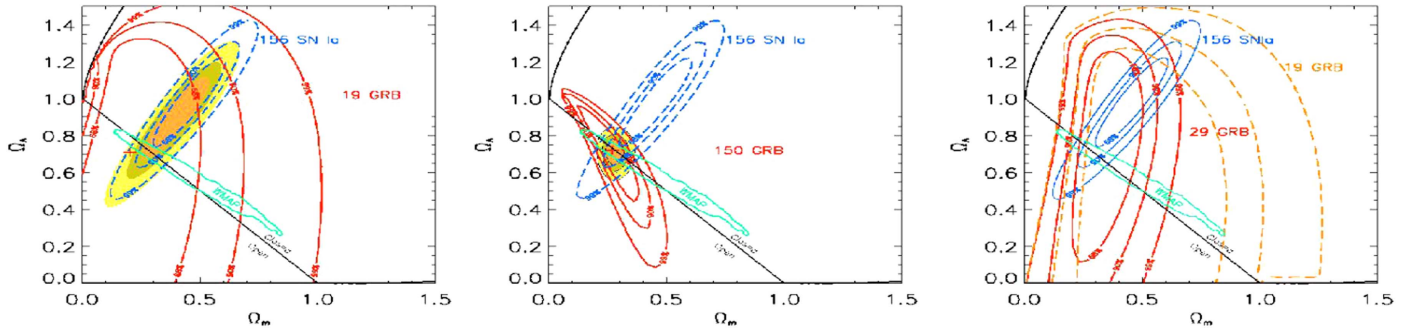

Figure 5. Left panel: the solid red contours, obtained with the samples of 19 alone, represent the 68.3%, 90% and 99% confidence regions of Ω_M and Ω_Λ obtained using the $E_{\rm peak} - E_\gamma$ in the HM case (Ghirlanda et al. 2006). The center of these contours (red cross) corresponds to a minimum $\chi 2$ and yields $\Omega_M = 0.23$, $\Omega_\Lambda = 0.81$. Middle panel: the same, but obtained with the sample of 150 GRBs simulated by assuming the $E_{\rm peak} - E_\gamma$ relation derived in the WM case (Ghirlanda et al. 2006). In both panels, the contours obtained with 156 SNe Ia of the "Gold" sample from (Riess et al. 2004) are shown by the dashed blue lines. The joint GRB +SN constraints are represented by the shaded contours. The 90% confidence contours obtained with the *WMAP* data are also shown. Right panel: the same, but obtained with the $E_{\rm peak} - E_\gamma$ relation updated until January 2009 (29 bursts—solid line; Ghirlanda 2009) compared with the previous data (19 GRBs—dashed line). The constraints obtained from 156 SN type Ia (blue thin line—Riess et al. 2004) and those from the *WMAP* data (green thin line) are also shown.

perform the calibration in a model-independent way might be developed using SNe Ia as a distance indicator based on a trivial observation that a GRB and a SN Ia with the same redshift z must have the same distance modulus $\mu(z)$. In this way GRBs should be considered complementary to SNe Ia at very high z, thus allowing to extend the distance ladder to much larger distances. Therefore, interpolation of the SNe Ia HD provides an estimate of $\mu(z)$ for a subset of the GRB sample with $z \leqslant 1.4$, which can then be used for calibration (Kodama et al. 2008; Liang et al. 2008; Wei & Zhang 2009). The modulus is given by the formula (Cardone et al. 2009)

$$\begin{aligned}\mu(z) &= 25 + 5\log D_L(z, \Omega_M, \Omega_\Lambda) \\ &= 25 + (5/2)(\log y - k) \\ &= 25 + (5/2)(a + b\log x - k)\end{aligned} \tag{11}$$

where $\log y = a + b\log x$, $y = kD_L^2(z, \Omega_M, \Omega_\Lambda)$ is a given quantity with k a redshift-independent constant, x is a distance-independent property, and a and b are the correlation parameters. With the assumption that this calibration is redshift-independent, the HD at higher z can be built with the calibrated correlations for the GRBs at $z > 1.4$ still present in the sample.

5.2. Applications of GRB Prompt Correlations

Dai et al. (2004) and Xu et al. (2005) proposed a method to constrain cosmological parameters using GRBs and applied it to preliminary samples (consisting of 12 and 17 events, respectively) relying on the $E_{\rm peak} - E_\gamma$ relation. They found $\Omega_M = 0.35^{+0.15}_{-0.15}$ (Dai et al. 2004) and $\Omega_M = 0.15^{+0.45}_{-0.13}$ (Xu et al. 2005) on 1σ CL, consistent with SNe Ia data.

Later, Ghirlanda et al. (2006) used 19 GRBs and claimed that the $E_{\rm peak} - E_\gamma$ and $E_{\rm peak} - E_{iso} - T_{\rm break}$ relations can be used to constrain the cosmological parameters in both the homogeneous (HM, see left panel in Figure 5) and wind circumburst medium (WM, see middle panel in Figure 5) cases. An updated sample of 29 GRBs (Ghirlanda 2009) allowed supporting previous results (see right panel in Figure 5).

However, to overcome the circularity problem affecting these correlations, Ghirlanda et al. (2006) considered three different methods to fit the cosmological parameters through GRBs:

(I) The scatter method based on fitting the correlation for a set of cosmological parameters that need to be constrained (e.g., Ω_M, Ω_Λ). To fulfill this task, a χ^2 surface in dependence on these parameters is built. The minimum of the χ^2 surface indicates the best cosmological model.

(II) The luminosity distance method consisting of the following main steps: (1) choose a cosmology (i.e., its parameters) and fit the $E_{\rm peak} - E_\gamma$ relation; (2) estimate the term $\log E_\gamma$ from the best fit; (3) from the definition of $\log E_\gamma$, derive $\log E_{\rm iso}$, from which $D_L(z, \Omega_M, \Omega_\Lambda)$ is next computed; and (4) evaluate χ^2 by comparing $D_L(z, \Omega_M, \Omega_\Lambda)$ with the one derived from the cosmological model. After iterating these steps over a set of cosmological parameters, a χ^2 surface is built. In this case, the best cosmology is represented also by the minimum χ^2.

(III) The Bayesian method: methods (I) and (II) stem from the concept that some correlation, e.g., $E_{\rm peak} - E_\gamma$, exists between two variables. However, these methods do not exploit the fact that the correlations are also very likely to be related to the physics of GRBs and, therefore, they should be unique. Firmani et al. (2005, 2006), employing the combined use of GRBs and SNe Ia, proposed a more complex method which considers both the existence and uniqueness of the correlation.

Another correlation that turns out to be useful in measuring the cosmological parameter Ω_M is the $E_{\rm peak} - E_{\rm iso}$ one (Amati et al. 2008). Adoption of the maximum likelihood approach provides a correct quantification of the extrinsic scatter of the correlation, and gives Ω_M narrowed (for a flat universe) to the interval 0.04–0.40 (68% CL), with a best-fit value of $\Omega_M = 0.15$, and $\Omega_M = 1$ is excluded at >99.9% CL. No specific assumptions about the $E_{\rm peak} - E_{\rm iso}$ relation are made, and no other calibrators are used for setting the normalization, therefore the problem of circularity does not affect the outcomes and the results do not depend on the ones derived from SNe Ia. The uncertainties in Ω_M and Ω_Λ can be greatly reduced, based on predictions of the current and expected GRB experiments.

An example of Bayesian method that takes into account the SNe Ia calibration is presented in Cardone et al. (2009). They updated the sample used in Schaefer (2007) adding to the previous 5 correlations the Dainotti relation $L_a - T_a^*$ (Dainotti et al. 2008). They used a Bayesian-based method for fitting and calibrating the GRB correlations assuming a representative ΛCDM model. To avoid the problem of circularity, local regression technique was applied to calculate $\mu(z)$ from the most recent SNe Ia sample containing (after selection cuts and having outliers removed) 307 SNe with $0.015 \leqslant z \leqslant 1.55$. Only GRBs within the same range of z defined by the SNe data were considered for calibration. It was shown that the estimated $\mu(z)$ for each GRB common to the (Schaefer 2007) and (Dainotti et al. 2008) samples is in agreement with that obtained using the set of Schaefer (2007) correlations. Hence, no additional bias is introduced by adding the $L_a - T_a^*$ correlation. In fact, its use causes the errors of $\mu(z)$ to diminish significantly (by ∼14%) and the sample size to increase from 69 to 83 GRBs.

Amati (2012) and Amati & Della Valle (2013) used an enriched sample of 120 GRBs to update the analysis of Amati et al. (2008). Aiming at the investigation of the properties of DE, the 68% CL contours in the $\Omega_M - \Omega_\Lambda$ plane obtained by using a simulated sample of 250 GRBs were compared with those from other cosmological probes such as SNe Ia, CMB, and galaxy clusters.

To obtain the simulated data set, Monte Carlo technique was employed. They took into account the observed z distribution of GRBs, the exponent, normalization and dispersion of the observed $E_{\rm peak} - E_{\rm iso}$ power-law relation, and the distribution of the uncertainties in the measured values of $E_{\rm peak}$ and $E_{\rm iso}$. The simulation showed that a sample of ≈250 GRBs is sufficient for the accuracy of Ω_M to be comparable to the one currently provided by SNe Ia. In addition, estimates of Ω_M and w_0 expected from the current and future observations were given. The authors assumed that the calibration of the $E_{\rm peak} - E_{\rm iso}$ relation is done with an accuracy of 10% using, e.g., the D_L provided by SNe Ia and the self-calibration of the GRB correlation via a sufficiently large number of GRBs within a narrow range of z (e.g., $\Delta z \sim 0.1$–0.2). It was also noted that as the number of GRBs in each redshift bin is increased, also the accuracy and plausibility of the $E_{\rm peak} - E_{\rm iso}$ relation's self-calibration should increase.

Tsutsui et al. (2009a) employed a sample of 31 low-z GRBs and 29 high-z GRBs to compare the constraints imposed on cosmological parameters (Ω_M and Ω_Λ) by i) the $E_{\rm peak} - T_L - L_{\rm peak}$ relation, and ii) the $L_{\rm peak} - E_{\rm peak}$ and $E_{\rm peak} - E_{\rm iso}$ relations calibrated with low-z GRBs (with $z \leqslant 1.8$; see left and middle panels in Figure 6, respectively). Assuming a ΛCDM model with $\Omega_k = \Omega_M + \Omega_\Lambda - 1$, where Ω_k is the spatial curvature density, it was found using the likelihood method that the constraints for the Amati and Yonetoku relations are different in 1σ, although they are still consistent in 2σ. Therefore, a luminosity time parameter, $T_L = E_{\rm iso}/L_{\rm peak}$, was introduced to correct the large dispersion of the $L_{\rm peak} - E_{\rm peak}$ relation. A new relation was given as

$$\log L_{\rm peak} = (49.87 \pm 0.19) + (1.82 \pm 0.08)\log E_{\rm peak} - (0.34 \pm 0.09)\log T_L. \quad (12)$$

The systematic error was successfully reduced by 40%. Finally, application of this new relation to high-z GRBs (i.e., with $1.8 < z < 5.6$) yielded $(\Omega_M, \Omega_\Lambda) = (0.17^{+0.15}_{-0.08}, 1.21^{+0.07}_{-0.61})$, consistent with the ΛCDM model (see right panel in Figure 7). The $\Omega_M - \Omega_\Lambda$ plane and the HD with the Amati relation are represented in the right and left panel of Figure 6.

Tsutsui et al. (2009b), using the $L_{\rm peak} - E_{\rm peak}$ relation, considered three cosmological cases: a ΛCDM model, a non-dynamical DE model ($w_a = 0$), and a dynamical DE model, viz. with $w(z) = w_0 + w_a z/(1+z)$, to extend the HD up to $z = 5.6$ with a sample of 63 GRBs and 192 SNe Ia (see Figure 8). It was found that the current GRB data are in agreement with the ΛCDM model (i.e., $\Omega_M = 0.28$, $\Omega_\Lambda = 0.72$, $w_0 = -1$, $w_a = 0$) within 2σ CL. Next, the constraints on the DE EoS parameters expected from *Fermi* and *Swift* observations were modeled via Monte Carlo simulations, and it was claimed that the results should improve significantly with additional 150 GRBs.

As shown by Tsutsui et al. (2011), with the use of the $E_{\rm peak} - T_L - L_{\rm peak}$ relation it is possible to determine the D_L with an error of about 16%, which might prove to be useful in unveiling the nature of DE at $z > 3$. In addition, it was pointed out in (Wang et al. 2011) that the correlations between the transition times of the X-ray light curve from exponential to power law, and the X-ray luminosities at the transitions such as the Dainotti et al. (2008) and the Qi & Lu (2010) correlations may be used as standard candles after proper calibration. This procedure, as explained by Wang et al. (2011), consists of a minimization of χ^2 (with the maximum likelihood method) over the parameters of the log-log relation (i.e., the slope and normalization), and simultaneously over the cosmological parameters. These relations can allow insight into cosmic

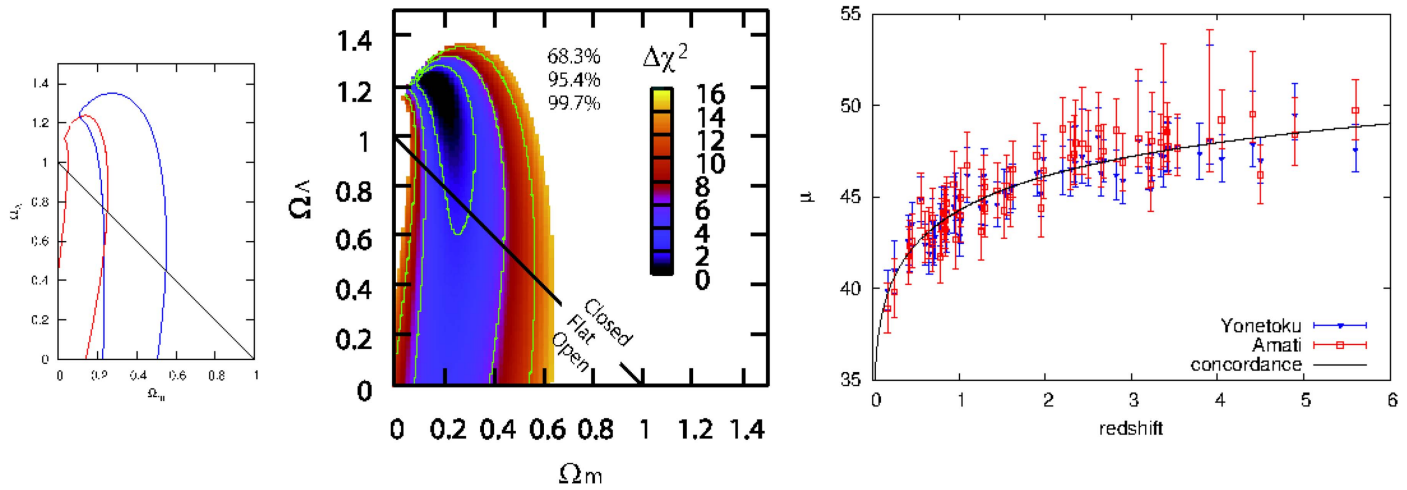

Figure 6. Left panel: constraints on Ω_M, Ω_Λ from the Amati (red) and Yonetoku (blue) relations (Tsutsui et al. 2009a). The contours correspond to 68.3% confidence regions; black solid line represents the flat universe. The results are consistent on the 2σ level. Middle panel: Constraints on Ω_M, Ω_Λ the from $E_{\rm peak} - T_L - L_{\rm peak}$ relation (Tsutsui et al. 2009a). Right panel: extended HD from the Amati (red) and Yonetoku (blue) relations (Tsutsui et al. 2009a). A systematic difference is apparent in high-z GRBs, although it does not seem to be present in low-z ones.

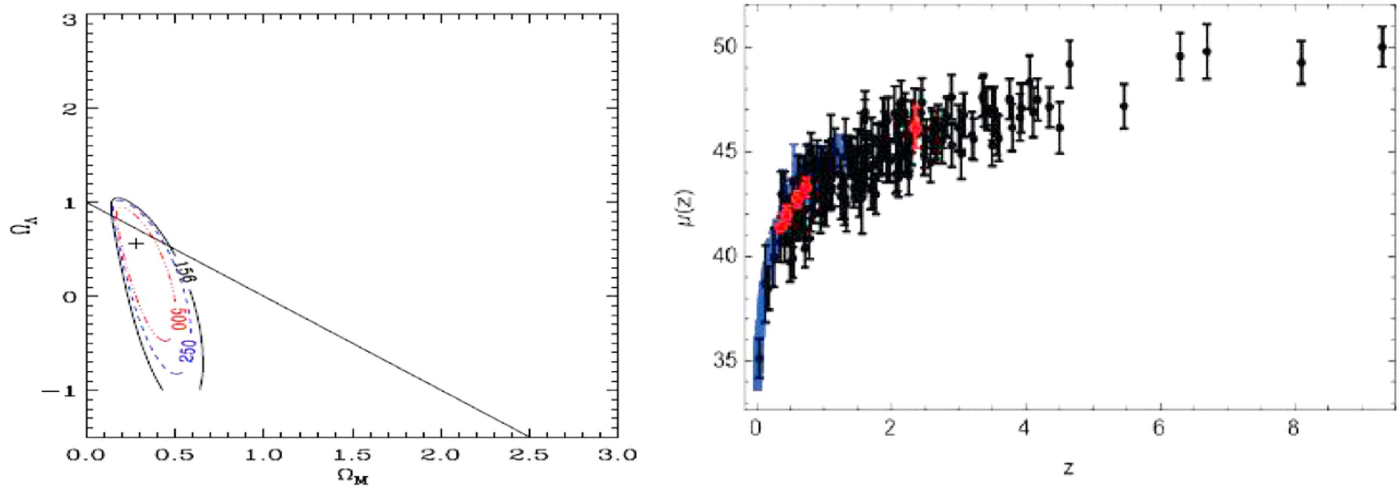

Figure 7. Left panel: 68% confidence level contour in the $\Omega_M - \Omega_\Lambda$ plane obtained by releasing the flat universe assumption with the sample of 156 GRBs available at the end of 2012 (black) compared with those expected in the next years with the increasing of GRBs in the sample (blue and red) with the Amati relation (Amati & Della Valle 2013). Right panel: GRB Hubble diagram (black points) is compared with the SN Ia Hubble diagram (blue points) and with BAO data (red points) from Demiański & Piedipalumbo (2015).

expansion at high z, and at the same time they have the potential to narrow the constraints on cosmic expansion at low z. GRBs could also probe the cosmological parameters to distinguish between DE and modified gravity models (Wang et al. 2009; Wang & Dai 2009; Vitagliano et al. 2010; Capozziello & Izzo 2008).

Lin et al. (2016) tested the possible redshift dependence of several correlations ($L_{\rm peak} - \tau_{\rm lag}$, $L_{\rm peak} - V$, $E_{\rm peak} - L_{\rm peak}$, $E_{\rm peak} - E_\gamma$, $L_{\rm iso} - \tau_{\rm RT}$, and $E_{\rm peak} - E_{\rm iso}$) by splitting 116 GRBs (with $z \in [0.17, 8.2]$ from Wang et al. 2011) into low-z (with $z < 1.4$) and high-z (with $z > 1.4$) groups. It was demonstrated that the $E_{\rm peak} - E_\gamma$ relation for low-z GRBs is in agreement with that for high-z GRBs within 1σ CL. The scatter of the $L_{\rm peak} - V$ relation was too large to formulate a reliable conclusion. For the remaining correlations, it turned out that low-z GRBs differ from high-z GRBs at more than 3σ CL. Hence, the $E_{\rm peak} - E_\gamma$ relation was chosen to calibrate the GRBs via a model-independent approach. High-z GRBs give $\Omega_M = 0.302 \pm 0.142$ (1σ CL) for the ΛCDM model, fully consistent with the Planck 2015 results (Planck and

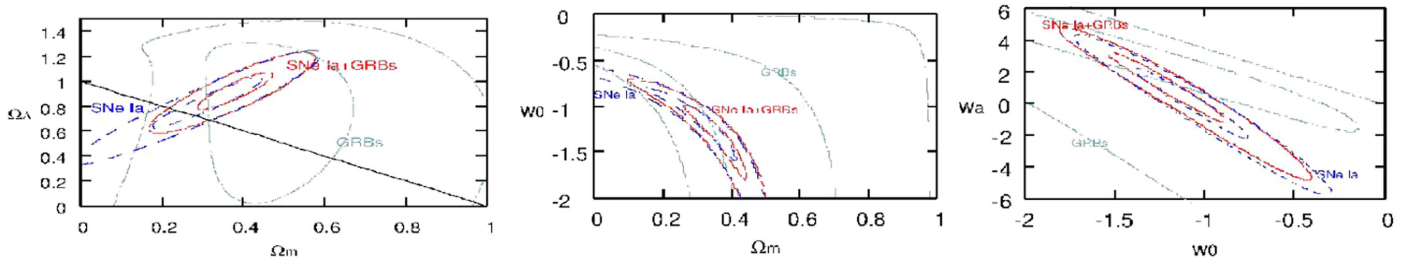

Figure 8. Contours of likelihood $\Delta\chi^2$ in (left panel) the (Ω_M, Ω_Λ), (middle panel) the (Ω_M, w_0), and (right panel) the 0(w_0, w_a) planes for GRBs (light blue dash-dotted lines), SNe Ia (blue dotted lines), SNe Ia+GRBs (red solid lines), respectively, from (Tsutsui et al. 2009b). The contours correspond to 68.3% and 99.7% confidence regions, and the black solid line represents the flat universe.

Fermi Collaborations et al. 2015). In conclusion, GRBs have already provided a direct and independent measurement of Ω_M, and simulations show that they will be able to achieve an accuracy comparable to SNe Ia.

5.3. Statistical Approaches Related to SNe Ia Cosmology

In the previous paragraphs we have identified the issue of GRBs not being easily standardizable into luminosity indicators, however to better employ GRBs for cosmology we here examine some of the more recent work in the field of Type Ia SN cosmology and the issues that are present in this field. This topic is relevant, because even in the application of SNe Ia, very popular standard candles, where the physical mechanisms of SNe Ia are well known, few issues with the statistical methods have been discussed recently in the literature. Therefore, for the application of GRBs as cosmological tools, where the physics of both the inner engine and of the afterglow is less understood, the statistical uncertainty is also larger, the instrumental selection effects can play a more relevant role on the results, and the sample size of luminosity indicators is smaller. Thus, we point out similarities and differences of standardization techniques and statistical procedures used for GRBs and SNe Ia and point out which methods used for SNe Ia maybe used for future directions on how to more effectively use GRBs as cosmological probes.

We here summarize several approaches employed to improve the constraints on cosmological parameters obtained from SNe Ia.

Mandel et al. (2009) constructed statistical models of SNe Ia Near Infrared (NIR) light curves, taking into account sources of randomness. Since NIR is more insensitive to dust extinction, this is a very promising approach. Indeed NIR luminosities form robust standard candles. Many light curve samples were used to average out randomized effects of different SNe. They attempted at selecting subsamples choosing data from objects that have less dust. Factors that distort inferences through reddening or dimming are indeed the dust, the intrinsic variation of the SNe light curves and their measurement errors. They employed hierarchical Bayes model for the creation of SNe Ia light curves in NIR, population distribution of intrinsic light curve variations and population distribution of dust. They used the Bayes theorem to create estimates for unknown parameters of individual SNe and overall population parameters. They employed a non-parametric approach, which does not try to characterize global behavior of light curves, but it features them locally, namely inferring local parameters within the light curves. This kind of approach can also help deal with missing data, infers them if there are gaps in temporal coverage and/or irregularities in the single light curves. Mandel et al. (2011) also used a hierarchical Bayesian approach to coherently model random effects on the redshift such as dust extinction, intrinsic light curve variations, and distances. They created predictive models of SNe Ia light curves in optical and near infrared. This work additionally improves upon the previous one laid out in Mandel et al. (2009) and uses an updated Markov Chain Monte Carlo algorithm that samples the global posterior probability density. The use of NIR and optical data combined together reduces further the contribution of the dust extinction and improves the predictive precision of individual SN Ia distances by about 60%. Using cross-validation, they calculated a distance modulus prediction error of 0.11 mag for SN with optical and NIR data versus 0.15 mag for SN with optical data exclusively. Therefore, continued study of SN Ia in the NIR is paramount for enhancing their usage as accurate cosmological distance indicators.

Differently from this approach, the one adopted for using GRBs as cosmological probes both in the prompt and in the afterglow features implies a Bayesian approach, such as the Reichart et al. (1999) or the D'Agostini (2005) method, but not a hierarchical approach. Thus, the intrinsic scatter is parametrized globally and there is no adoption of a non-parametric approach. Instead, the hierarchical model incorporates randomness and uncertainties due to measurement errors, intrinsic SN variations, dust extinction, and reddening, peculiar velocities and distances into parametric inferences about individual SN and the population. The parameters describing the population of SN Ia light curves, include also intrinsic variations and correlations in shape, color, and luminosity across multiple

wavelengths. The dust population parameters rule the population distribution of host galaxy dust values. Each SN randomly draws dust parameters from this distribution. These dust parameters are combined with the individual absolute light curves and distance modulus to generate an apparent light curve modeled with noise to reproduce the observed multi-wavelength light curve. In the close universe, μ is a function of the redshift through the Hubble law plus a noise term representing random peculiar velocities of host galaxies. This random process is conceptually repeated for each SN in the data set. The difference between the distance prediction and the training set of the SNe Ia light curves relies on the fact that the first does not influence the redshift-distance likelihood information of the SNe.

Also in March et al. (2011) a Bayesian hierarchical model is used to ensure better constraints on the cosmological parameters from SNe Ia data obtained with the SALT-II light-curve fitter. They further used simulated data to indicate that their methodology brings tighter statistical constraints on the cosmological parameters by reducing statistical bias typically by a factor of 2–3. Moreover, in this study a full posterior probability distribution for the dispersion of the intrinsic magnitude of SNe is obtained. This method applied to the latest SNe Ia data together with BAO and CMB led to $\Omega_M = 0.28 \pm 0.02$, $\Omega_\Lambda = 0.73 \pm 0.01$ under the assumption of $w = -1$ and to $\Omega_M = 0.28 \pm 0.01$, $w = -0.90 \pm 0.05$ under the assumption of flatness. Further, upon constraining the B-band magnitude of the SNe Ia intrinsic dispersion, they obtained $\sigma_\mu = 0.13 \pm 0.01$ mag.

Shariff et al. (2016) analyzed through a BAyesian Hier-Archical Modeling for the Analysis of Supernova cosmology (the BAHAMAS software) 740 SNe Ia from the data set of the "Joint Light-curve Analysis" (JLA). They simultaneously determined cosmological parameters combining JLA and Planck CMB data and they discovered substantial discrepancies in cosmological parameters compared with the standard analysis: $\Omega_M = 0.399 \pm 0.027$, $w = -0.910 \pm 0.045$, 2.8σ and 1.6σ higher than previous estimates. They investigated if this discrepancy could be determined by the existence of two sub-populations possessing different host galaxy masses and by a sudden 4σ difference of the color correction parameter at a $z = 0.662$. Neither of these two events cause these discrepancies, thus leaving this problem still an open issue.

Thus, the additional work of Rubin et al. (2015) examine the limitations that characterize the present SNe cosmological approaches, when it comes to outlier treatment, selection effects, heterogeneous observations, intrinsic dispersion, shape, and color standardization associations. They offer a novel Bayesian model, known as UNITY (Unified Nonlinear Inference for Type Ia cosmologY), that integrates substantial enhancements in dealing with those effects. They applied the model to real SNe observations showing that the results give smaller statistical and systematic uncertainties. They validated previous results that SNe Ia require nonlinear shape and color standardizations, however they included these nonlinear relations in a statistical way that is well-justified. This analysis was blinded, because the validation of method was first on simulated data, and no analysis changes were made after repeating the same procedure with real data.

Nielsen et al. (2016) investigate the validity of the "standard" model of cosmology by using the currently much bigger database of SNe Ia compared with the ones used to estimate the accelerated expansion rate of the universe. With the nowadays database of SNe Ia it is possible to rigorously statistically test whether these "standardizable candles" probe the cosmic acceleration. Taking account the empirical procedure by which corrections to their absolute magnitudes are applied to allow for the variation of the shape of the light curve and extinction by dust, they found surprisingly almost a constant rate of expansion. This shows only a marginal evidence for the acceleration.

From this wide panorama, it is clear that another probe at much higher redshift as GRBs can help to cast light on the discrepancies mentioned in March et al. (2011) and on the investigation of the acceleration of the expansion as discussed in Nielsen et al. (2016). To this end, we would need to improve the methodology of using GRBs as cosmological tools to have a precision cosmology comparable with the ones obtained by the SNe Ia. Future missions have among others this challenging goal, such as SVOM (Cordier et al. 2015) and Theseus.

We now compare and contrast the analysis performed for cosmology for the GRB analysis. First, GRBs have circularity problem that need to be avoided using cosmology-independent variables, while for the SNe Ia the Cepheid variables are used as good calibrators in the same galaxy and where there are more low-z SNe Ia to observe. Thus, for the SNe Ia the calibration is not as much of a concern. In addition, differently from the non-parametric approach of Mandel et al. (2011), the method used for GRBs is parametric through well-known relations and single light curves are not taken into account. To model the light curves in a non-parametric way one has to model the shape of the light curves locally, describing the variations in signal in each neighborhood of phase and wavelength, to build up a model for the light curve over the full range of phase and wavelength. The probabilistic hierarchical approach also provides a principled framework for dealing with missing data. In the GRB analysis there has not been developed yet methods to treat with missing data regarding the construction of the GRB prompt emission relations, thus this can create bias effects. It is advisable that this probabilistic approach will be applied to GRBs, because the local modeling will provide better estimate of the parameters. The dust extinction are modeled already in the computation of the light curves and they are not parameters in the hierarchical model, indeed the light curve in the *Swift*

repository are already unabsorbed; for details of how these light curves were produced, see Evans et al. (2009). In addition, the intrinsic scatter for the GRB analysis is modeled parametrically. In addition, in the GRB analysis a training set among the GRB light curves has not been identified yet. The gold sample of flat plateaus (Dainotti et al. 2016b) without the other categories (Dainotti et al. 2017) can be a crucial tool to define a good training set among GRB light curves for implementing the method described for SNe Ia to GRBs instead.

6. Summary

In this work, we reviewed the characteristics of empirical relations among the GRB prompt phase observables, with a particular focus on the selection effects, and we discussed possible applications of several correlations as distance indicators and cosmological probes. It is crucial that a number of the correlations face the problem of double truncation which affects, e.g., the value of $E_{\rm peak}$. Some relations have also been shown to be intrinsic in nature (e.g., the $E_{\rm peak} - F_{\rm tot}$, $E_{\rm peak} - E_{\rm iso}$, or $L_{\rm peak} - E_{\rm peak}$ ones), while the intrinsic forms are not known for others. As a consequence, we are not yet aware whether these correlations can affect the evaluation of the theoretical models of GRBs and the cosmological setting (Dainotti et al. 2013a). Therefore, establishing the intrinsic correlations is crucial. In fact, though there are several theoretical interpretations describing each correlation, in many cases more than one is viable, thus showing that the emission processes that rule GRBs still have to be further investigated. To this end, it is necessary to use the intrinsic correlations, not the observed ones that are affected by selection biases, to test the theoretical models. A very challenging future step would be to use the correlations corrected for biases to determine a further and more precise estimate of the cosmological parameters.

M.G.D. acknowledges the Marie Curie Program, because the research leading to these results has received funding from the European Union Seventh Framework Program (FP7-2007/2013) under grant agreement No. 626267. M.G.D. is particular grateful to Roberta del Vecchio and Mariusz Tarnopolski for their preliminary work on this review.

References

Amati, L. 2006, MNRAS, 372, 233
Amati, L. 2012, International Journal of Modern Physics Conf. Ser., 12, 19
Amati, L., & Della Valle, M. 2013, IJMPD, 22, 1330028
Amati, L., Frontera, F., Tavani, M., et al. 2002, A&A, 390, 81
Amati, L., Guidorzi, C., Frontera, F., et al. 2008, MNRAS, 391, 577
Amati, L., Frontera, F., & Guidorzi, C. 2009, A&A, 508, 173
Andreon, S. 2013, in Astrostatistical Challenges for the New Astronomy, ed. J. M. Hilbe (New York: Springer), 41
Atteia, J.-L. 2003, A&A, 407, L1
Azzam, W. J. 2012, IJAA , 2, 1
Band, D., Matteson, J., Ford, L., et al. 1993, ApJ, 413, 281
Band, D. L., & Preece, R. D. 2005, ApJ, 627, 319
Bégué, D., & Pe'er, A. 2015, ApJ, 802, 134B
Bevington, P. R., & Robinson, D. K. 2003, Data Reduction and Error Analysis for the Physical Sciences (New York: McGraw-Hill)
Bosnjak, Z., Celotti, A., Longo, F., & Barbiellini, G. 2008, MNRAS, 384, 2
Bošnjak, Ž., Götz, D., Bouchet, L., Schanne, S., & Cordier, B. 2014, A&A, 561, A25
Burgess, J. M., Ryde, F., & Yu, H.-F. 2015, MNRAS, 451, 1511
Butler, N. R., Kocevski, D., & Bloom, J. S. 2009, ApJ, 694, 76
Capozziello, S., & Izzo, L. 2008, A&A, 490, 31
Cardone, V. F., Capozziello, S., & Dainotti, M. G. 2009, MNRAS, 400, 775
Cavallo, G., & Rees, M. J. 1978, MNRAS, 183, 359
Collazzi, A. C., Schaefer, B. E., & Moree, J. A. 2011, ApJ, 729, 89
Collazzi, A. C., Schaefer, B. E., Goldstein, A., & Preece, R. D. 2012, ApJ, 747, 39
Cordier, B., Wei, J., Atteia, J. L., et al. 2015, in PoS. Conf. Proc., Swift: 10 Years of Discovery (arXiv:1512.03323)
Costa, E., Frontera, F., Heise, J., et al. 1997, Natur, 387, 783
Cucchiara, A., Levan, A. J., Fox, D. B., et al. 2011, ApJ, 736, 7
D'Agostini, G. 2005, Fits, and especially linear fits, with errors on both axes, extra variance of the data points and other complications. *ArXiv Physics e-prints*,
Dai, Z. G., Liang, E. W., & Xu, D. 2004, ApJL, 612, L101
Dainotti, M., Petrosian, V., Willingale, R., et al. 2015a, MNRAS, 451, 3898
Dainotti, M., Del Vecchio, R., & Tarnopolski, M. 2018, AdAst, 2018, 4969503
Dainotti, M. G., Cardone, V. F., & Capozziello, S. 2008, MNRAS, 391, L79
Dainotti, M. G., Willingale, R., Capozziello, S., Fabrizio Cardone, V., & Ostrowski, M. 2010, ApJL, 722, L215
Dainotti, M. G., Fabrizio Cardone, V., Capozziello, S., Ostrowski, M., & Willingale, R. 2011, ApJ, 730, 135
Dainotti, M. G., Cardone, V. F., Piedipalumbo, E., & Capozziello, S. 2013a, MNRAS, 436, 82
Dainotti, M. G., Petrosian, V., Singal, J., & Ostrowski, M. 2013b, ApJ, 774, 157
Dainotti, M. G., Del Vecchio, R., Nagataki, S., & Capozziello, S. 2015b, ApJ, 800, 31
Dainotti, M. G., Postnikov, S., Hernandez, X., & Ostrowski, M. 2016, ApJL, 825, 20
Dainotti, M. G., Nagataki, S., Maeda, K., Postnikov, S., & Pian, E. 2017, Å, 600, 98
Della Valle, M., Malesani, D., Benetti, S., Chincarini, G., Stella, L., & Tagliaferri, G. 2006, IAU Circ., 8696, 1
Demiański, M., & Piedipalumbo, E. 2015, ARep, 59, 484
Dichiara, S., Guidorzi, Amati, L. C., & Frontera, F. 2013, MNRAS, 431, 3608
Efron, B., & Petrosian, V. 1992, ApJ, 399, 345
Efron, B., & Petrosian, V. 1998, arXiv:astro-ph/9808334
Evans, P. A., Beardmore, A. P., Page, K. L., et al. 2009, MNRAS, 397, 1177
Fishman, G. J., Meegan, C. A., Wilson, R. B., et al. 1994, ApJS, 92, 229
Firmani, C., Ghisellini, G., Ghirlanda, G., & Avila-Reese, V. 2005, MNRAS, 360, L1
Firmani, C., Avila-Reese, V., Ghisellini, G., & Ghirlanda, G. 2006, MNRAS, 372, L28
Ford, L. A., Band, D. L., Matteson, J. L., et al. 1995, ApJ, 439, 307
Frontera, F., Amati, L., Guidorzi, C., Landi, R., & in't Zand, J. 2012, ApJ, 754, 138
Fynbo, J. P. U., Watson, D., Thöne, C. C., et al. 2006, Natur, 444, 1047
Galama, T. J., Vreeswijk, P. M., van Paradijs, J., et al. 1998, Natur, 395, 670
Gehrels, N., Chincarini, G., Giommi, P., et al. 2005, ApJ, 621, 558
Ghirlanda, G. 2009, in AIP Conf. Ser., Vol. 1111, ed. G. Giobbi et al. (Melville, NY: AIP), 579
Ghirlanda, G., Ghisellini, G., & Lazzati, D. 2004, ApJ, 616, 331
Ghirlanda, G., Ghisellini, G., & Firmani, C. 2005, MNRAS, 361, L10
Ghirlanda, G., Ghisellini, G., & Firmani, C. 2006, NJPh , 8, 123
Ghirlanda, G., Nava, L., Ghisellini, G., Firmani, C., & Cabrera, J. I. 2008, MNRAS, 387, 319
Ghirlanda, G., Nava, L., Ghisellini, G., Celotti, A., & Firmani, C. 2009, A&A, 496, 585
Ghirlanda, G., Nava, L., & Ghisellini, G. 2010, A&A, 511, A43
Ghirlanda, G., Ghisellini, G., & Nava, L. 2012, MNRAS, 422, 2553
Goldstein, A., Preece, R. D., & Briggs, M. S. 2010, ApJ, 721, 1329

Golkhou, Z. V., & Butler, N. 2014, ApJ, 787, 90
Golkhou, Z. V., Butler, N., Littlejohns, J., & Owen, M. 2015, ApJ, 811, 93
Greiner, J., Mazzali, P. A., Kann, D. A., et al. 2015, Natur, 523, 189
Guiriec, S., Daigne, F., Hascoet, R., et al. 2013, ApJ, 770, 1
Guiriec, S., Gonzalez, M. M., Sacahui, J. R., et al. 2016a, ApJ, 819, 79
Guiriec, S., Kouveliotou, C., Hartmann, D. H., et al. 2016b, ApJL, 831, L8
Heise, J., Zand, J. I., Kippen, R. M., & Woods, P. M. 2001, in Gamma-ray Bursts in the Afterglow Era, ed. E. Costa, F. Frontera, & J. Hjorth, 16
Heussaff, V., Atteia, J.-L., & Zolnierowski, Y. 2013, A&A, 557, A100
Hjorth, J., Sollerman, J., Møller, P., et al. 2003, Natur, 423, 847
Horváth, I. 1998, ApJ, 508, 757
Kaneko, Y., Preece, R. D., Briggs, M. S., et al. 2006, ApJS, 166, 298
Kendall, M., & Stuart, A. 1973, The Advanced Theory of Statistics. Vol. 2: Inference and Relationship (3rd ed.; London: Griffin), 1973
Kippen, R. M., Woods, P. M., Heise, J., et al. 2001, in Gamma-ray Bursts in the Afterglow, ed. E. Costa, F. Frontera, & J. Hjorth, 22
Klebesadel, R. W., Strong, I. B., & Olson, R. A. 1973, ApJL, 182, L85
Kocevski, D. 2012, ApJ, 747, 2
Kocevski, D., & Petrosian, V. 2013, ApJ, 765, 116
Kodama, Y., Yonetoku, D., Murakami, T., et al. 2008, MNRAS, 391, L1
Kouveliotou, C., Meegan, C. A., Fishman, G. J., et al. 1993, ApJL, 413, L101
Kumar, P., & Zhang, B. 2015, PhR, 561, 1
Lee, T. T., & Petrosian, V. 1996, ApJ, 470, 479
Li, L.-X., & Paczyński, B. 2006, MNRAS, 366, 219
Liang, E., & Zhang, B. 2005, ApJ, 633, 611
Liang, E., & Zhang, B. 2006, MNRAS, 369, L37
Liang, N., Xiao, W. K., Liu, Y., & Zhang, S. N. 2008, ApJ, 685, 354
Lin, H.-N., Li, X., Wang, S., & Chang, Z. 2015, MNRAS, 453, 128
Lin, H.-N., Li, X., & Chang, Z. 2016, MNRAS, 455, 2131
Lloyd, N. M., & Petrosian, V. 1999, ApJ, 511, 550
Lloyd, N. M., Petrosian, V., & Mallozzi, R. S. 2000, ApJ, 534, 227
Lu, R.-J., Wei, J.-J., Liang, E.-W., et al. 2012, ApJ, 756, 112
Malesani, D., Tagliaferri, G., Chincarini, G., et al. 2004, ApJL, 609, L5
Mallozzi, R. S., Paciesas, W. S., Pendleton, G. N., et al. 1995, ApJ, 454, 597
Mandel, K. S., Narayan, G., & Kirshner, R. P. 2011, ApJ, 731, 120
Mandel, K. S., Wood-Vasey, M., Friedman, A. S., & Kirshner, R. P. 2009, ApJ, 704, 629
March, M. C., Trotta, R., Berkes, P., et al. 2011, MNRAS, 418, 4
Mazets, E. P., Golenetskii, S. V., Ilinskii, V. N., et al. 1981, Astrophysics and Space Science, 80, 3
Mochkovitch, R., & Nava, L. 2015, A&A, 577, A31
Mészáros, P. 2006, Rep. Prog. Phys., 69, 2259
Mészáros, P., Rees, M. J., & Wijers, R. A. M. J. 1998, ApJ, 499, 301
Mukherjee, S., Feigelson, E. D., Babu, G. J., et al. 1998, ApJ, 508, 314
Nakar, E., & Piran, T. 2005, MNRASL, 360, 1
Nava, L., Salvaterra, R., Ghirlanda, G., et al. 2012, MNRAS, 421, 1256
Nielsen, D., Guffanti, A., Sarkar, A., et al. 2016, ApJ, 35596, 6
Norris, J. P., & Bonnell, J. T. 2006, ApJ, 643, 266
Norris, J. P., Nemiroff, R. J., Bonnell, J. T., et al. 1996, ApJ, 459, 393
Norris, J. P., Marani, G. F., Bonnell, J. T., et al. 2000, ApJ, 534, 248
O'Brien, P. T., Willingale, R., Osborne, J., et al. 2006, ApJ, 647, 1213
Perley, D. A., Perley, R. A., Hjorth, J., et al. 2015, ApJ, 801, 102
Petrosian, V., Kitanidis, E., & Kocevski, D. 2015, ApJ, 806, 44
Petrosian, V., Singal, J., & Stawarz, L. 2013, In Multi- wavelength AGN Surveys and Studies, volume 9 of Proceedings of the International Astronomical Union, 10 pages, http://journals.cambridge.org/article_S174392131400369X
Pian, E., D'Avanzo, P., Benetti, S., et al. 2017, Natur, 551, 67
Planck and Fermi Collaborations, Ade, P. A. R., Aghanim, N., et al. 2015, A&A, 582, A31
Qi, S., & Lu, T. 2010, ApJ, 717, 1274
Rea, N., Gullon, M., Pons, J. A., et al. 2015, ApJ, 813, 92
Reichart, D. E., Castander, F. J., & Nichol, R. C. 1999, ApJ, 516, 1
Reichart, D. E., Lamb, D. Q., Fenimore, E. E., et al. 2001, ApJ, 552, 57
Rhoads, J. E. 1997, ApJL, 487, L1
Riess, A. G., Strolger, L.-G., & Tonry, J. 2004, ApJ, 607, 665
Rodney, S. A., Riess, A. G., Scolnic, D. M., et al. 2015, AJ, 150, 156
Rowlinson, A., Gompertz, B. P., Dainotti, M., et al. 2014, MNRAS, 443, 1779
Rubin, D., Aldering, G., Barbary, K., et al. 2015, ApJ, 813, 2
Ryde, F., & Svensson, R. 2002, ApJ, 566, 210
Sakamoto, T., Hill, J. E., Yamazaki, R., et al. 2007, ApJ, 669, 1115
Sari, R., Piran, T., & Halpern, J. P. 1999, ApJL, 519, L17
Schaefer, B. E. 2007, ApJ, 660, 16
Schulze, S., Malesani, D., Cucchiara, A., et al. 2014, A&A, 566, A102
Shahmoradi, A. 2013, ApJ, 766, 111
Shahmoradi, A., & Nemiroff, R. J. 2015, MNRAS, 451, 126
Shariff, H., Jiao, X., Trotta, R., & van Dyk, D. A. 2016, ApJ, 827, 1
Sparre, M., Sollerman, J., Fynbo, J. P. U., et al. 2011, ApJL, 735, L24
Spearman, C. 1904, The American Journal of Psychology, 15, 72
Stern, B. E., & Svensson, R. 1996, ApJL, 469, L109
Tarnopolski, M. 2015a, A&A, 581, A29
Tarnopolski, M. 2015b, MNRAS, 454, 1132
Troja, E., Cusumano, G., O'Brien, P. T., et al. 2007, ApJ, 665, 599
Tsutsui, R., Nakamura, T., Yonetoku, D., et al. 2008, in American Institute of Physics Conference Series, volume 1000 of American Institute of Physics Conference Series, ed. M. Galassi, D. Palmer, & E. Fenimore, 28 pages
Tsutsui, R., Nakamura, T., Yonetoku, D., et al. 2009a, Journal of Cosmology and Astro-Particle Physics, 8, 015
Tsutsui, R., Nakamura, T., Yonetoku, D., et al. 2009b, MNRAS, 394, L31
Tsutsui, R., Nakamura, T., Yonetoku, D., Murakami, T., & Takahashi, K. 2011, PASJ, 63, 741
Tsutsui, R., Yonetoku, D., Nakamura, T., Takahashi, K., & Morihara, Y. 2013, MNRAS, 431, 1398
van Paradijs, J., Groot, P. J., Galama, T., et al. 1997, Natur, 386, 686
Vitagliano, V., Xia, J.-Q., Liberati, S., & Viel, M. 2010, Journal of Cosmology and Astro-Particle Physics, 3, 005
Wang, F. Y., & Dai, Z. G. 2009, MNRAS, 400, L10
Wang, F. Y., Dai, Z. G., & Qi, S. 2009, A&A, 507, 53
Wang, F.-Y., Qi, S., & Dai, Z.-G. 2011, MNRAS, 415, 3423
Wei, H., & Zhang, S.-N. 2009, European Physical Journal C, 63, 139
Wijers, R. A. M. J., Rees, M. J., & Meszaros, P. 1997, MNRAS, 288, L51
Willingale, R., O'Brien, P. T., Osborne, J. P., et al. 2007, ApJ, 662, 1093
Willingale, R., Genet, F., Granot, J., & O'Brien, P. T. 2010, MNRAS, 403, 1296
Woosley, S. E., & Bloom, J. S. 2006, Annual Review of Astronomy and Astrophysics, 44, 507
Xu, D., Dai, Z. G., & Liang, E. W. 2005, ApJ, 633, 603
Yonetoku, D., Murakami, T., Nakamura, T., et al. 2004, ApJ, 609, 935
Yonetoku, D., Murakami, T., Tsutsui, R., et al. 2010, PASJ, 62, 1495
Zhang, B., & Mészáros, P. 2001, ApJL, 552, L35
Zhang, B., & Mészáros, P. 2002, ApJ, 581, 1236
Zhang, B.-B., Liang, E.-W., & Zhang, B. 2007, ApJ, 666, 1002
Zitouni, H., Guessoum, N., Azzam, W. J., & Mochkovitch, R. 2015, Astrophysics and Space Science, 357, 7